CHALMERS

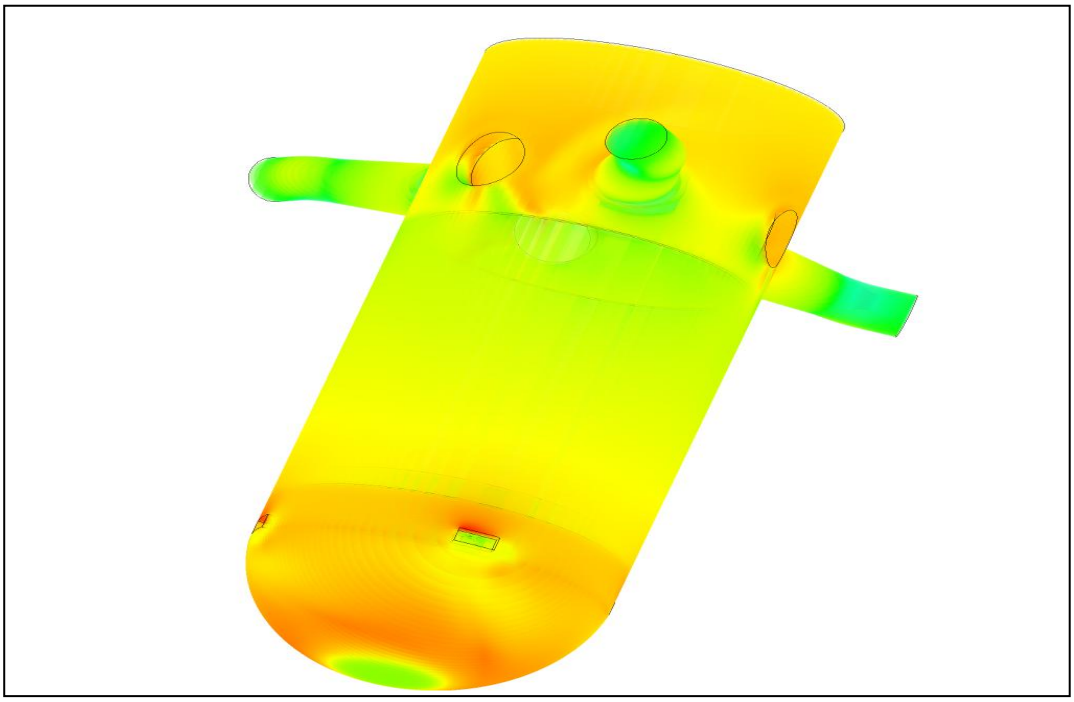

Pressure pulses measurements as a way of determining reactor core barrel movements

Master of Science Thesis [Nuclear Engineering, TIFX03]

CHRISTOFFER NORDSTRÖM

Department of Applied Physics
Division of Nuclear Engineering
CHALMERS UNIVERSITY OF TECHNOLOGY
Gothenburg, Sweden, 2012

CTH-NT-258 ISSN 1653-4662

Pressure pulses measurements as a way of determining reactor core barrel movements

Master of Science Thesis
Master's Programme in Nuclear Engineering
CHALMERS UNIVERSITY OF TECHNOLOGY

CHRISTOFFER NORDSTRÖM

Department of Applied Physics
Division of Nuclear Engineering
CHALMERS UNIVERSITY OF TECHNOLOGY
Gothenburg, Sweden, 2012

Pressure pulses measurements as a way of determining reactor core barrel movements
Master of Science Thesis
CHRISTOFFER NORDSTRÖM

CTH-NT-258
ISSN 1653-4662
Department of Applied Physics
Division of Nuclear Engineering
CHALMERS UNIVERSITY OF TECHNOLOGY
Gothenburg, Sweden, 2012

Cover:
Volume rendering of absolute pressure in a reactor pressure vessel

Chalmers Reproservice
Gothenburg, Sweden 2012

Abstract

This work investigates if a movement of the core barrel in a pressurized water reactor may give rise to pressure pulses inside the reactor pressure vessel. The results are then evaluated with regards to which positions ~~it~~ would be best suitable to measure said pressure pulsation. The investigation is meant to conclude if it is plausible to use these pulsations to determine if the lower radial supports are working properly, securing the core barrel in place, stopping it from vibrating/moving. The lower supports have a maximum allowed gap between the clevis insert ant the lower radial support, this gap is known to be larger than intended but still below the upper allowed limit. If the gap would grow as large as it is allowed, would it should then be possible to measure this from the core barrel vibrations made possible from this gap. There are only certain positions where these measurements can be done, is it possible to se pressure pulses at these positions? From an initial heavily simplified model this seems to be the case, forcing vibrations with a certain frequency of the core barrel gives rise to a small fluctuation of about 0.009 MPa at the locations of interest. These pulsations show an almost linear relation between the core barrel displacement and peak to peak pressure amplitude. A more detailed model was used for the final simulation. This model confirms the results from the simplified model, showing a slightly larger pressure pulse in several of the guide tube positions. The peak to peak amplitude is about 0.002 MPa. The maximum fluctuations are occurring close to the periphery of the reactor pressure vessel, with both of the models. This suggests that it would be beneficial to measure the fluctuations at such a position.

Keywords: CFD, vibrations, lower radial supports, pressure pulses, PWR

Acknowledgements/Preface

This work is done as a M.Sc. thesis and has been written for Ringhals AB with via Epsilon. I would like to thank Jenny Roudén and Mats Olmeby at Ringhals and Per Löfquist at Epsilon for their help and support. Further I would like thank Carl Stenson for his support regarding CFX. Finally I would like to thank Epsilon and Ringhals for the opportunity to do this thesis for them.

Göteborg, June 2012
Christoffer Nordström

Table of contents

Lift of abbreviations

LWR	- Light Water Reactor
PWR	- Pressurized Water Reactor
BWR	- Boiling Water Reactor
CFD	- Computational Fluid Dynamics
CFX	- Ansys® CFX
RC-Flow	- Reactor Coolant Flow
PRZ	- Pressurizer
RPV	- Reactor Pressure Vessel
LES	- Large Eddy Simulation
DNS	- Direct Numerical Simulation
N-S	- Navier-Stookes
SS	- Steady State
AR	- Aspect ratio

Nomenclature

ρ	- Density [$kg\ m^{-3}$]
g	- Gravitational constant [ms^{-2}]
$\dot{m}$	- Mass flow [$kg\ s^{-1}$]
c_p	- Specific heat capacity [$J\ kg^{-1}K^{-1}$]
k	- Thermal conductivity [$W\ m^{-1}K^{-1}$]
β	- Thermal expansion coefficient [K^{-1}]
$\boldsymbol{u}$	- Vector velocity [$m\ s^{-1}$]
u, v, w	- Velocity components [$m\ s^{-1}$]
S	- Source term
μ	- Dynamic viscosity [$Pa\ s$]
υ	- Kinematic viscosity [$m^2 s^{-1}$]
Φ	- Dissipation function [J m^{-3}]
p	- Pressure [Pa]
i	- Internal energy [$J\ kg^{-1}$]
Re	- Reynolds Number
Co	- Courant Number
U	- Velocity [$m\ s^{-1}$]
$\overline{U}$	- Time averaged velocity [$m\ s^{-1}$]
u	- Fluctuating velocity component [$m\ s^{-1}$]
τ	- Shear Stress [Nm^{-1}]
k	- Turbulent kinetic energy [$m^2 s^{-2}$]
ε	- Turbulent dissipation [$m^2 s^{-3}$]
τ_w	- Wall shear stress [Nm^{-1}]
S	- Arc length [m]
r	- Radius [m]
θ	- Angular component in cylindrical coordinate system [rad]

y_{barrel} - Core barrel radius $[m]$

y_{disp} - Core barrel displacement $[m]$

H_{barrel} - Core barrel height $[m]$

f - Core barrel frequency $[HZ]$

1. Introduction

~~In the following chapter a short description of the project background, also the problem, purpose and aim will be presented. A short overview of nuclear power will also be presented.~~

A nuclear reactor generates heat from nuclear fission which is then used to boil steam for electricity production. The most common reactors in use today are light water reactors (LWR), in these reactors the coolant, ordinary (light) water is used as both the moderator and coolant. [1] A moderator is a material, fluid or solid that moderates the fast neutrons generated by fission and slows them down. The slowed down neutrons, usually called thermal neutrons have a higher probability to cause fission in the fuel(usually enriched uranium or a mix of enriched uranium and plutonium) Heat is generated by the fission caused by thermal neutrons, boiling water either directly or via primary and secondary water loops. In boiling water reactors (BWR), a type of LWR the coolant is boiled directly in the core. In the case of pressurized water reactors (PWR) the steam is boiled in a secondary loop which is connected to the primary one via heat exchangers, see figure 1. In PWR: s the coolant is subjected to high pressure, keeping the coolant liquid all the time inside the core. The steam drives a turbine which then in turn drives a turbine generating electricity to the grid. [2]

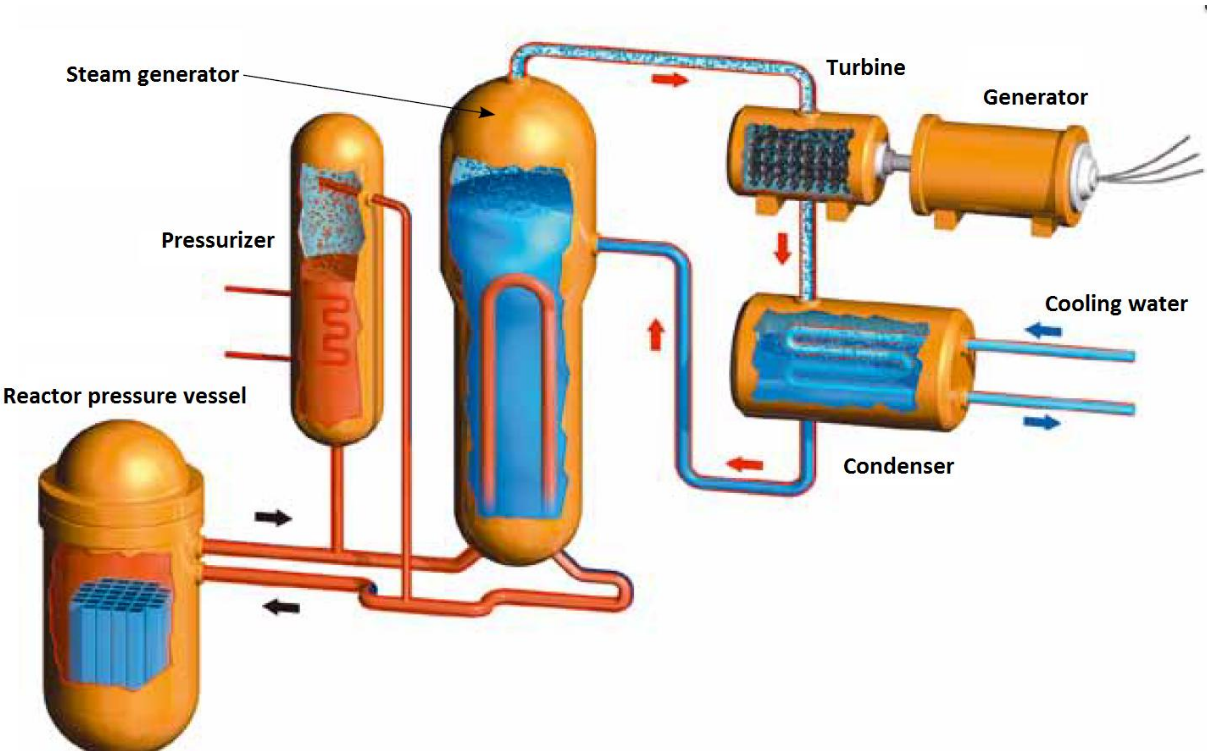

Figure 1: Overview of electricity generation with a PWR [5]

Due to low interest in nuclear power under many years, not many new reactors has been built under later years, making it important to keep the old ones running. [3] In the case of Sweden most reactors were built during the 1970-1980. In later years the wish to extend the operation of these reactors beyond the designed life raises makes it more important to keep track of wear and other age related problems. [4]

This work is going to investigate the plausibility of indirectly measuring small movements/vibrations of the internal parts in a nuclear reactor by monitoring the pressure. The motion is believed to occur due to an increased gap in the lower radial supports. It is theorized that it may be possible to get an indication of this motion by looking at the pressure variations at a specific location in the reactor. The motion and gap in the lower radial supports is of interest due to safety concerns and risk of breakages during unexpected events. If these gaps get to large the vibrations may cause damage to other parts of the reactor.

The reason for the interest in the core barrel motion is to determine the gap in the lower radial supports since this is a parameter used in many safety investigations, both the motion itself and the gap size is thus of interest. The vibration is believed to be occurring when the core barrel is not securely fastened in the bottom. This motion if occurring should then generate small pressure pulses inside the reactor pressure vessel (RPV). It would then be possible to measure these pulses and try to determine how much the core barrel is moving. The amplitude of the core barrel motion is limited by the gap in the lower radial supports, thus the vibration should in theory be able to give an indication of the state of the lower radial supports.

The reactor concerned in this work is located at Ringhals Nuclear power plant. This site has four reactors in operation three of which are Pressurized water reactors (PWR), units 2-4 and one Boiling Water Reactor (BWR) unit 1. This project focuses on Ringhals 2 (R2) of type PWR. R2 was commissioned as the first of four reactors at the site on 1 May, 1975 [5]. The R2 unit is of Westinghouse 3-loop PWR design which is shown in figure 2. The reactor is designed with an outer shell, the reactor pressure vessel and internal parts, core barrel that distribute the main coolant flow and hold the core. The core barrel which is the main internal part is supported in the top by reactor vessel flange, and by guides, lower radial supports, in the bottom. The core barrel is being subjected to flow induced forces from the reactor coolant flow (RC-flow) that after long term operation has generated increased gaps, due to wear, in the lower radial supports. These increased gaps are believed to allow for certain unwanted vibration of the core barrel.

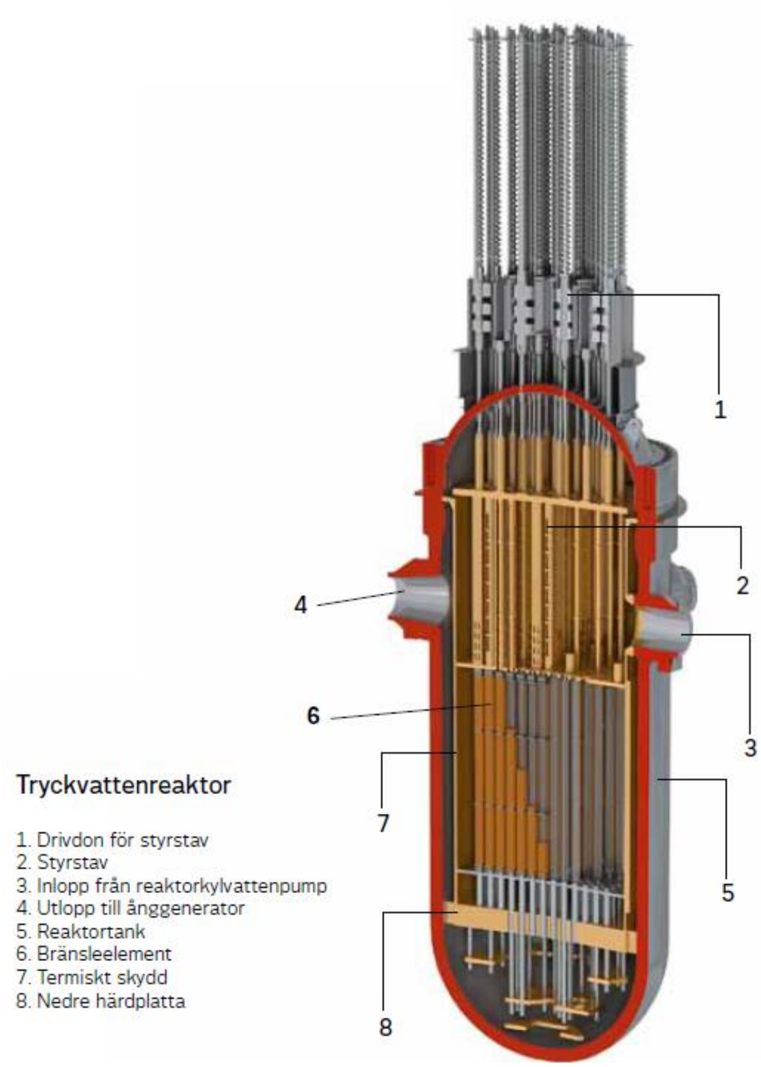

Figure 2: Illustration of a typical PWR [6]

1.1. Background

The reactor construction, for the scope of this work, is described as a pressure vessel with internal parts that distribute the main coolant flow and carry the core. The core barrel which is the main internal part is supported in the top by reactor vessel flange and in the bottom by the lower radial supports. The lower radial supports consists of two main parts, a Clevis key and a Clevis Insert. These lower supports (See **1.** in figure 3) guides the reactor vessel lower internals in the reactor pressure vessel. There are four lower radial supports spaced 90° in-between se figure 4 and 5.

It has been observed, after long term operation, that gaps has appeared at the lower radial supports in the Reactor vessel on Ringhals 2-4 (PWR) due to wear. The wear appears on the Clevis inserts and radial key, see arrows in figure 5. When the tolerances in the lower radial supports increase, the core barrel can move to a greater extent than initially intended. Today, the maximum allowable gaps (tolerances) are 1 mm on each side of a support. The area subjected to wear is marked in figure 5.

The lower radial supports are supposed to guide the reactor core barrel in its tangential direction whilst still allowing it to expand in both axial and radial direction. The supports were designed with a small tolerance which has since grown due to wear. This added gap makes it possible for the core barrel to move/vibrate more than what it was intended to.

It has not been determined if the wear is ongoing or if it is something that has been happening in the past. The wear causes no direct safety concern as is today but may pose an availability risk of the reactor in the future. If the wear gets to large the core barrel can move to a greater extent causing greater loading on different parts of the reactor. This may in extreme cases lead to breakages during unexpected events etc. A larger wear may also invalidate safety studies. It is thus important to continuously keep track of this wear.

It is not possible to directly measure the wear during operation. It is however possible to measure the gaps when the reactor is stopped and the core barrel and the reactor vessel can be disassembled. This has proven to be a complex and time consuming procedure which is only done every couple of years. Thus it would be desirable to get some indication of the state of these supports by indirect measurements from available operational parameters.

It has been theorized that it could be possible to measure pressure pulses in the core coolant to use as an indicator of core barrel movement. The movements of the core barrel may compress the coolant at certain locations inside the reactor giving rise to a fluctuation of pressure. These measurements could then be performed during operation and give an indication vibration of the core barrel and thus the state of the supports. The theory is that there will be pressure pulses appearing when the core barrel moves that then propagates through the reactor coolant. It may thus be possible to measure these pulses in other points of the reactor. There may however be many sources of pressure pulses as well as many components obstructing the path of these pulses before they can be measured. It is thus far from certain that the pressure pulses measured actually originates from core barrel movements and not from something else. It is thus important to measure the pressure pulses as close to the source as possible.

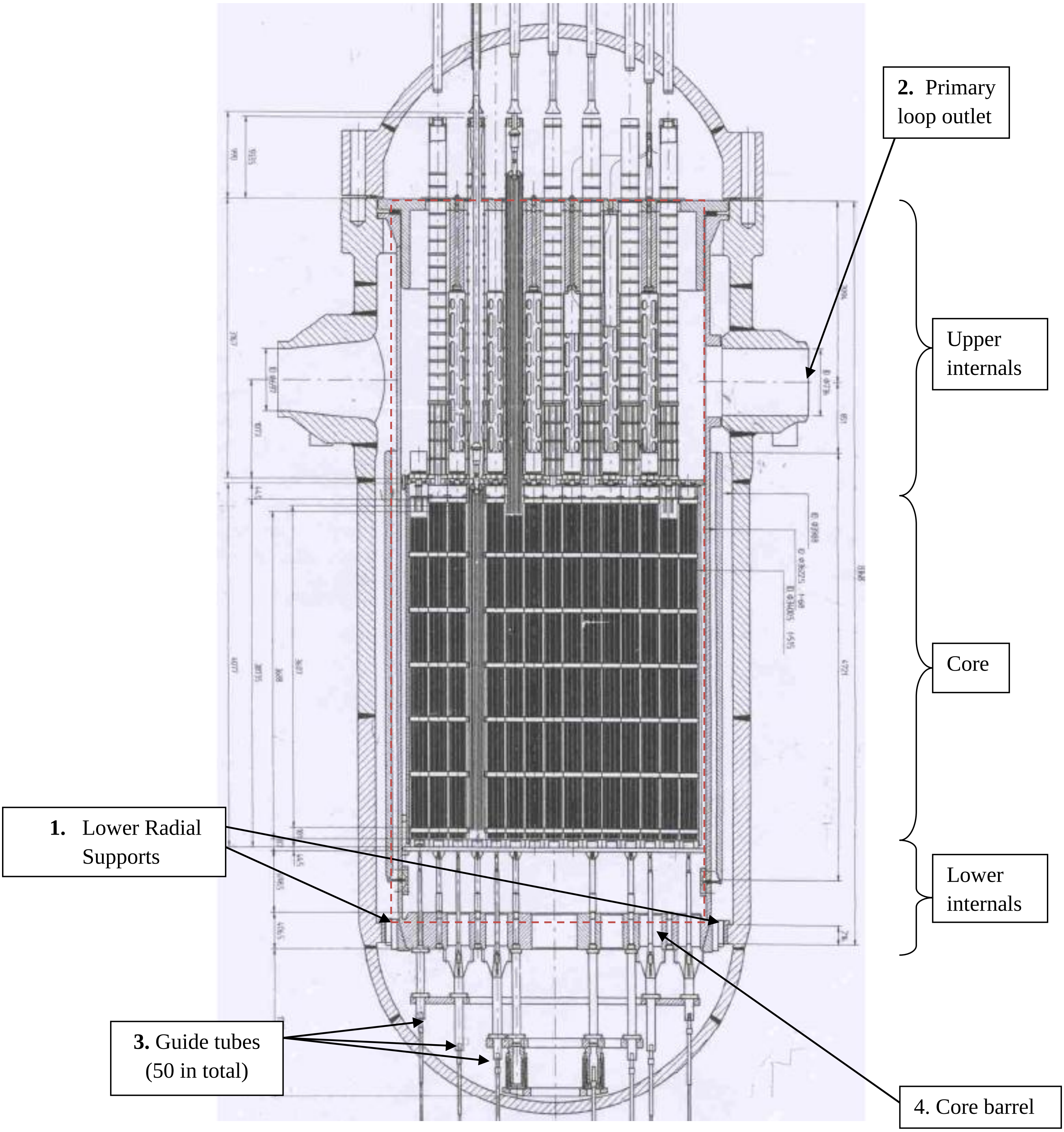

Figure 3: Schematic of Ringhals R2 PWR Reactor

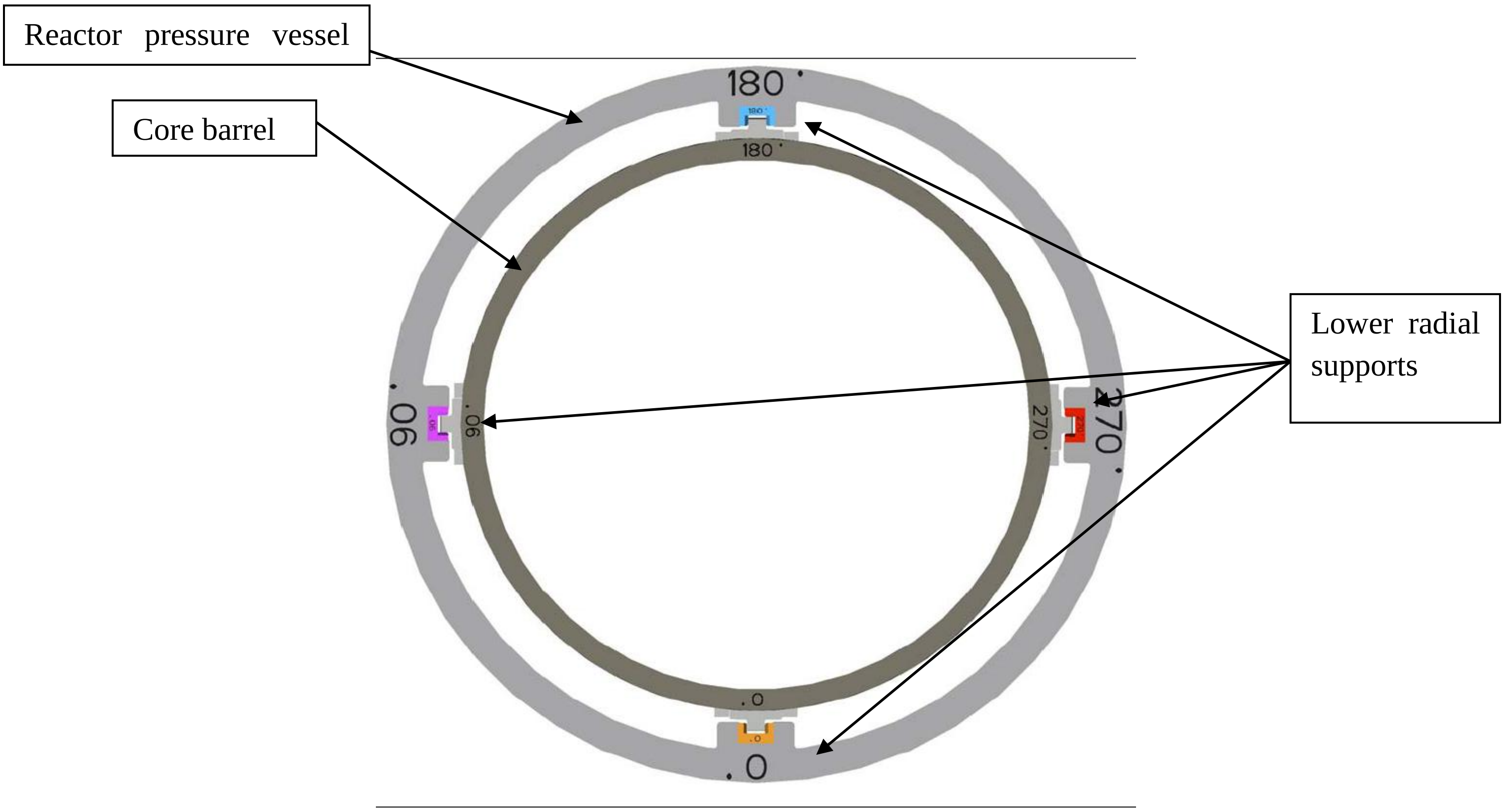

Figure 4: Illustration of lower radial supports

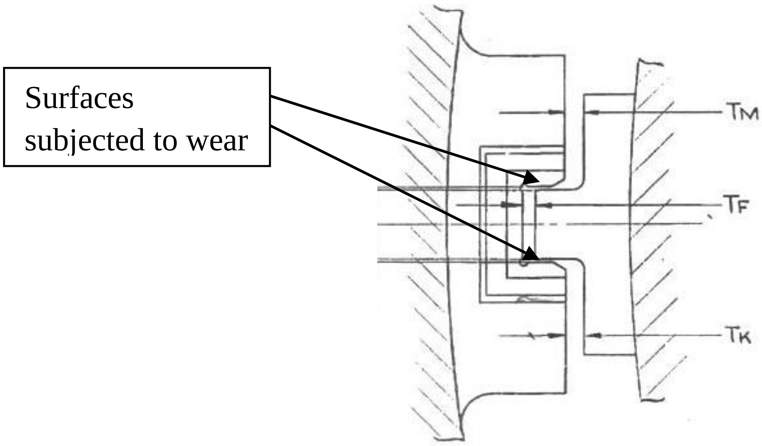

Figure 5: Lower radial support seen from above

There are only a few places where measurements of the pressure are possible. Mainly points 2 and 3 in figure 3. The guide tubes in point 3 actually consists of several possible positions where to take measurements. The guide tubes are mainly used for core measurements such as neutron flux etc. In R2 some of these tubes are not used leaving room for one or several pressure sensors. These tubes are designed to guide a measuring probe inside the reactor to the core. The guide tubes extends for several tens of meters outside the core and are filled with water, see figure 6 below. The tubes leads to a seal table were its possible to insert the measurements probes. From the beginning all of these tubes were used for guiding sensors for measuring core-parameters, however during later re-design some of these tubes were no longer needed and was subsequently plugged at the seal table.

These plugged guide tubes may be used to measure the pressure inside the reactor vessel. Measurements can and has been performed by replacing the plug at the seal table with a pressure sensor. Attaching the sensor at the seal table gives the pressure pulses a long way to travel before reaching the sensor, it is however not possible/allowed to insert the pressure sensors directly into the pressure vessels as done with core-sensors since they are not designed to accommodate sensors of these type.

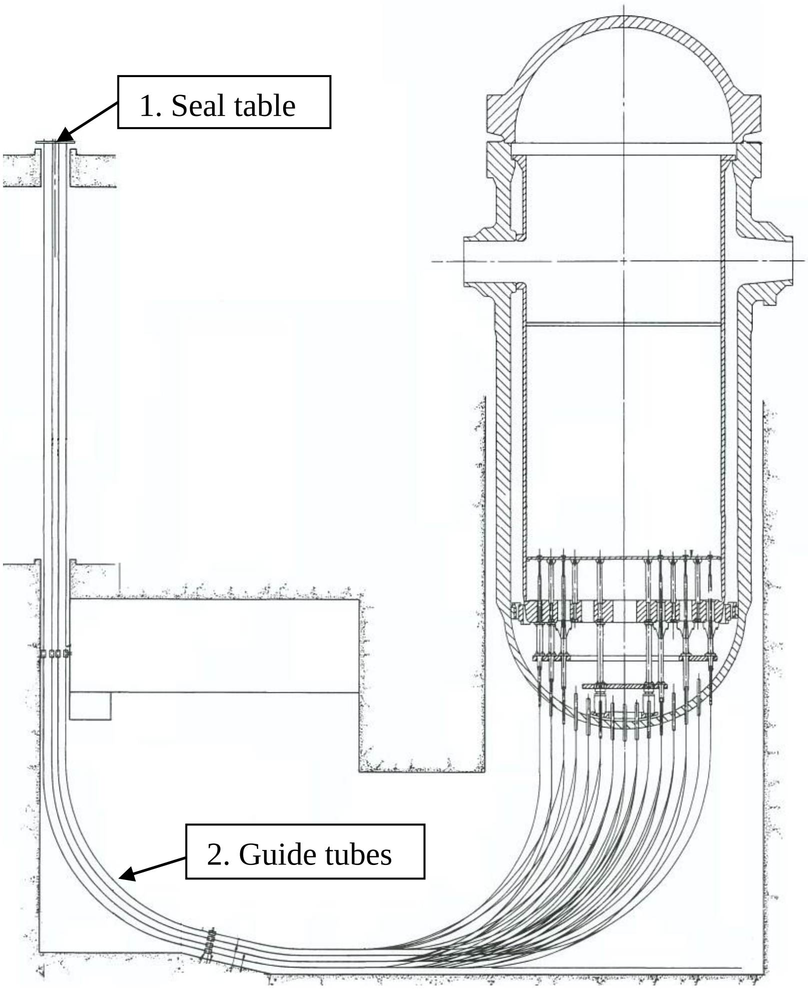

Figure 6: Reactor pressure vessel with guide tubes and seal table

1.2. Purpose and Aim

The aim of this thesis work is to determine if the possible motion/vibration of the reactor core barrel inside the reactor pressure vessel (RPV) gives rise to pressure pulses at the locations mentioned earlier. Does a motion small enough to still be within allowable limits give rise to any substantial and measurable change in pressure? Since a larger motion of the core barrel is only made possible with an increased gap at the lower radial supports the motion should give an indication of the state of these supports. If the pressure changes noticeably from a motion smaller than is possible with the maximum allowed wear on the lower radial supports, the pressure may be used as an indication of the state of these.

Measurements of the pressure pulses have been performed in the primary loop and in one of the guide tubes on R2. The results have so far not been evaluated to such an extent that it is possible to determine if there is a relation between measured pressure pulses and an increased movement of the core barrel. The signal shows many peaks at several different frequencies and amplitudes. Some of these may be explained by other phenomena. The blades on the pump wheels for example may give rise to peaks with the same frequency as the blade rotation. It is thus important to know what to look for in such signals.

Summarized the main issues to be evaluated:

- Does movement of the core barrel give rise to pressure pulses at the points of interest?
- Is a motion restricted by the maximum increased gap at the lower radial supports large enough to give any noticeable pressure pulses?
- Which of the measuring points would be best suited for the detection of the possible pressure pulses?

1.3. Boundaries

This work will be limited to determine the plausibility of using this kind of measurements to determine lower radial support wear. Neither the actual wear nor type of movement of the core barrel is going to be evaluated.

Only R2 is modeled and studied. The results from the R2-model should be comparable to the other two PWR units at Ringhals which are of similar design.

A very simple reactor model will be used were the reactor is considered to consist of an outer pressure vessel and the main internal parts and lower radial supports. All other internal components will be neglected. Further vibrations from pumps and other components will also be neglected. There are many different parts in the reactor that may obstruct the pulses from the movements as well as create pressure pulses themselves, the influence of these will be neglected. Factors as dampening of the water and other parts will be neglected.

The possible movements of the core barrel will not be analyzed but instead an imposed movement will be used in the model. This is the movement that is theorized to be happening inside the reactor, due to the location it is however some uncertainty. Further only the two measuring points used for the real pressure pulse measurements will be evaluated. The movement modeled will be a simple pendulum movement of the core barrel with a given frequency and amplitude. Although the core barrel vibrates/moves in a lot of different directions, this part of the motion is believed to be the one that contributes the most to the theoretical pressure pulses.

The model is going to be used to see if there is a measurable pressure pulse at the locations of interest ~~and~~ will not predict the actual shape or amplitude of such a pulse. If there is measurable pressure pulses at these points the best possible guide tube for making these measurements will be evaluated.

Further it is not possible to have the measurement probes directly at the locations stated earlier. Instead the probes are fastened on the guide tube seal-table that in some cases is separated by up to 30 meters long guide tubes. In figure 6 below the reactor pressure vessel together with the guide tubes and seal table is shown. These tubes are filled with water and may cause problems with resonances etc. These problems however will be neglected in this work. Instead the model produced will evaluate the actual (simulated) pressures at the other end of these tubes neglecting what may or may not happen on its way through the tubes.

2. Method

The first step in this thesis work will be a literature study in order to find out if something similar has been done before. Is there work going on in this subject and show is it progressing. If it has been done before, what were the results? If there has been significant work done previously it may be possible to learn from this? The literature study is supposed to evaluate if a simulation of this kind is possible without becoming too complex for the scope of this thesis. The literature study would later show that there is little work done concerning pressure pulses as a gauge for motion or vibration in a reactor setting. The results from the literature will therefore mainly concern the validity of Computational fluid dynamics (CFD) for simulations of PWR: s and the main assumptions used, the findings can be found in chapter 3.1.

A simple model of the reactor vessel and some parts of the main coolant loops is to be done with commercial CFD software, trying to get simulated measurements of the pressure in the points of interest. The model is supposed to be a simplified model, to narrow down parameters affecting the pulses and the desired measurements. The model and mesh will be constructed in the commercial meshing software Beta CAE Systems ANSA and the CFD-simulations will be conducted in ANSYS® CFX software.

By keeping the model as simple as possible it should be possible to determine what parts of the measured pressure pulses that are actually originating from the core barrel movements. By imposing a motion on the core barrel and solving for the pressure in the measuring points available. The simulation would then show how the pressure pulses at the possible measuring points. The possible fluctuations created by the motion of the core barrel may be dampened along the way when the fluid path is obstructed. By comparing the results from the model with only the components of interest it will be possible to see if some part of the measured pressure pulse originates from these movements.

The model will be constructed incrementally with complexity added in each version. This is done so that errors in the model and their sources can be more easily identified as well as avoiding unnecessary complexity if no significant pressure variation will occur.

First a steady state simulation of the simplified geometry is performed, trying to get a good mesh and sufficient mesh resolution. Several steady state simulations with different meshes will be performed and evaluated against each other. The mesh with the lowest resolution that still gives satisfactory accuracy will then be used for the transient solution.

Further a simulation with a very simple geometry will be done to evaluate problems with the motion in particular, making it easier to find errors. The simulation will first be run without any flow calculations (de-activating corresponding equations in CFX) to determine if the motion of the core barrel is as expected. Secondly a simulation with flow is solved for a very large motion; this is done to determine if a larger motion gives any pressure rise in the system. If this is the case a second simulation is run, with the maximum allowable amplitude.

It should then be possible to combine the two input and results from these runs in a final simulation. The steady-state solution together with the motion settings will be used together to give a transient simulation of the geometry in question.

From these simulations it should then be possible to determine if a motion of the core barrel with the maximum magnitude allowed will give rise to a large enough pressure fluctuations to be measured.

Simulations will be performed on two different geometries, one heavily simplified model, referred to as "simplified model" and a second more accurate model referred to as “full model” that supposed to predict the flow more accurately called "full model". The simulations that are going to be performed on these two models are listed in table 1.

Table 1: Simulations to be performed

Simplified model:
1. Steady-state (SS) simulation(s) a. *Should give a starting point for subsequent simulations with the simplified geometry*. 2. Transient simulation with mesh motion without solving the flow a. *Should show that the motion of the core barrel works as intended.* 3. Transient simulations with 10mm amplitude a. *Should show if a low resolution mesh is able to pick up fluctuations in pressure from small motions.* b. *Should give an indication of god measurement positions.* c. *Should show if it’s worth going on with the full simulations.* 4. Transient simulations with pressure inlet and mass flow inlet boundary with 0.5, 1, 2.5, 5, 10 and 15 mm motion amplitude. a. *Should check boundary condition sensitivity.* b. *Determine pressure versus displacement behavior* c. *Should give an indication of the pressure amplitude to be expected from the full simulation.*
Full model:
1. SS simulations on the full model with different meshes making sure of mesh-independent solutions. a. *Should make sure that the flow is accurately determined in the reactor.* 2. Final transient simulation of the full model and 1mm motion amplitude. a. *Should give the final support for measurement recommendations.*

From these simulations, the pressure at the location of the guide tube openings inside the reactor will be measured as a function of time. Having several measuring points at the different locations available for measuring should give an indication of witch location is most suitable to detect the highest pressure variation for a given motion. The guide tubes open up inside the reactor and are threaded inside a larger hollow tube guiding the probe the last bit up into the core. Since this opening is the largest opening between the tube interior and the reactor pressure vessel this is where the general pressure inside the reactor core is believed to influence that of the guide tubes, see red circles in figure 7. Position 2 in figure 3 will not be treated here; the reasons for this will be treated in the results and conclusions chapters.

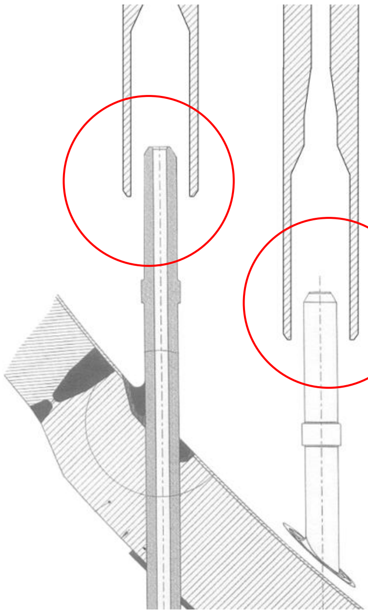

Figure 7: Guide tube openings

3. Theory

A PWR is a type of nuclear reactor where the coolant is subjected to high pressure to keep it in liquid form, even at the high temperatures present inside the reactor. Generally the pressure inside a PWR is about 15.5 MPa and a temperature of around 300 ℃. The fact that the coolant is in liquid form makes it easier to model because two phase-flows is avoided.

Since there are movements of the core barrel and the 3-loop PWR is not symmetric, a model that is capable of handling 3-dimensional systems is needed. Because of this CFD is chosen to simulate the system. CFD is a way of numerically solving complex flow systems by discretizing the fluid domain into small volumes by finite volume methods. Using equations for Continuity, momentum and energy it is possible to solve the flow iteratively. This way of solving the flow however is an approximation and not an exact method.

The main approximation done in CFD is the use of finite elements, where properties are averaged over small volumes and time averaging for turbulence. Further approximations for the fluid behavior, such as incompressibility are usually assumed.

The continuity equation states that the mass in a volume is conserved. Figure 8 below show what flows in and out a small fluid element. This can be expressed in vector notation as in equation 3.1 below. [7]

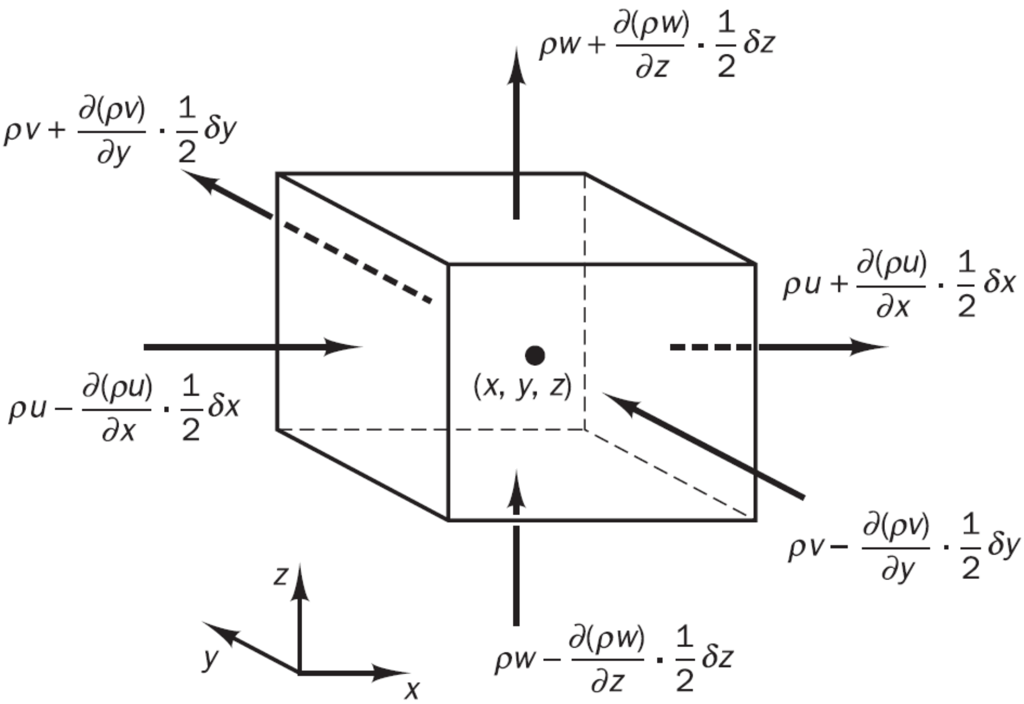

Figure 8: Mass flow through a fluid element, [7]

Further equations for momentum and energy are needed and can be seen in equations 3.2 – 3.6. Where S is a source term and Φ is a dissipation function. [7]

continuity:

$$\frac{\partial \rho}{\partial t} + div(\rho \boldsymbol{u}) = 0 \tag{3.1}$$

x-momentum:

$$\frac{\partial(\rho u)}{\partial t} + div(\rho u \boldsymbol{u}) = \frac{\partial p}{\partial x} + div\big(\mu\, grad(u)\big) + S_{Mx} \tag{3.2}$$

y-momentum:

$$\frac{\partial(\rho v)}{\partial t} + div(\rho v \boldsymbol{u}) = \frac{\partial p}{\partial y} + div\big(\mu\, grad(v)\big) + S_{My} \tag{3.3}$$

z-momentum:

$$\frac{\partial(\rho w)}{\partial t} + div(\rho w \boldsymbol{u}) = \frac{\partial p}{\partial x} + div\big(\mu\, grad(w)\big) + S_{Mz} \tag{3.4}$$

energy:

$$\frac{\partial(\rho i)}{\partial t} = div(\rho i \boldsymbol{u}) = -p\, div(\boldsymbol{u}) + div\big(k\, grad(T)\big) + \Phi + S_i \tag{3.5}$$

equations of state:

$p = p(\rho, T)$ and $i = i(\rho, T)$ (3.6)

3.1. Validation of CFD simulations

There are often questions about the validity of CFD-models since it's an approximate method. Therefore it is important to validate the results obtained from such models. In the case of this work real validation will not be possible. It would be both very complex and expensive to do experimental test. Instead this model is meant as a plausibility study of measuring pressure pulses from core-barrel motion/vibration.

However there have been several other studies which have compared CFD-simulations of reactor core flows and transients against experimental data. One such study is a reactor core transient simulation of a VVER-1000 reactor performed by Böttcher. [8] Using a very simplified model of a transient in the reactor where the heat up in one of the primary coolant loops due to isolation of one turbine was simulated. The results of the simulation of this study showed of generally good agreement with measured data. There was however some cases where 1st order models better predicted the flow behavior then 2nd order schemes. This difficulty was mainly in predicting the temperature and heat flow which in this work is neglected. The study also concluded that the reactor geometry needs to be heavily simplified in order to make it plausible to perform transient CFD-simulations.

The main simplification done in the study mention above that is of interest in this work:

- Solids neglected because energy content of steel structures is much larger than for that of the coolant
- Outer boundaries are considered adiabatic
- Some design elements only considered by pressure losses
- Smaller components are strongly simplified

Several other studies, where the flow and different transients where studied have come to similar conclusions. [9], [10], [11] One study was regarding vibration of the core barrel, with high frequency. The study compared CFD simulations with experimental data on a Japanese APWR reactor. This study was regarding higher vibration frequencies than in this work which lead them to use LES as the turbulence model. LES turbulence models do not use any time approximation which makes it suitable when treating high frequency vibration. The study showed of good accuracy between CFD-simulations and experimental data. [12]

One problem in particular seems to be resolving y^+. This is a dimensionless variable used to determine the flow behavior close to the wall and is dependent on the distance of the closest node to the wall. Without an adequate y^+ the boundary layer isn't resolved and the accuracy of the solution is reduced.

3.2. Treating motions in CFD simulations

For a transient problem such as this, where movement involved there are three common methods of treating motion in CFD-simulations. These methods are described in table 2 below. [13]

Table 2: The main different mesh motion treatment methods [12]

Mesh-less methods	An approximate method that do not use the Navier-Stookes (N-S) equations, instead it uses the viscosity as a way of modeling the motion and is thus of limited use in this work.
Fixed-mesh methods Implemented in Ansys® CFX as "Immersed Solids"	The fixed mesh works by solving the N-S equations on a stationary mesh with the boundaries moving relative to the mesh. This method is sometimes called immersed boundary method.
M**oving-mesh methods** Implemented in Ansys® CFX as "Deforming meshes"	The mesh-less method is Finally the moving-mesh method applies the motion directly to the mesh itself. This is done by deforming the mesh is such a way that the boundaries move as desired. This way of moving the boundaries gives rise to finite node-velocities which has to be accounted for in the governing equation.

Fixed mesh methods is able to handle complex flow geometries past several bodies. They do however require complex algorithms for mesh moving boundary tracking making it computationally expensive. Another drawback is that it requires a very fine mesh over the whole area to be spanned by the moving boundary to keep mesh-resolution high enough at all times. [13]

The body fitted moving mesh method alleviates many of the problems experienced by the fixed mesh approach by moving the mesh along with the body. This is done by deforming the mesh in such a way that the desired motion is achieved. Moving the mesh in this way makes the mesh-resolution of the boundary satisfactory for the whole motion and allows for body fitted meshes. The major drawback of this method is the required re-meshing at each time step, adding computational time to the transient simulation. Another downside is that this method cannot handle complex translational and rotational movements. [13]

Given the limitations of the imposed motion in the form of a pendulum motion, the body fitted moving mesh is going to be used in the following simulations. Since the motion is simple and the amplitude of the movement is low a moving mesh method will be the most beneficial motion treatment for the problem at hand.

3.3. Turbulence models

The flow in a nuclear reactor is highly turbulent. Turbulence gives small fluctuations in the flow in both time and space. Turbulence is highly unsteady and consists of many scales. This makes it necessary to impose simplifications to take into account these fluctuations in a manner that is realistic in regards to computational resources required. These simplifications impose small errors compared to the real flow; different models threat turbulence differently and are better to predict certain flow behaviors but worse at others. Therefore it is important to choose the right turbulence model for the problem in particular. If a flow is laminar or turbulent is determined by the Reynolds number which is defined in equation 3.7. [14]

$$Re = \frac{\rho V L}{\mu} = \frac{VL}{\nu} \tag{3.7}$$

There exist many schemes for treating turbulent flow, the most common ones are direct numerical simulation DNS, k- ε, k- ω and Large eddy simulation LES.

The Mesh is very important for turbulence modeling and CFD in general, especially when direct numerical simulation is used (DNS). In DNS all eddies in the turbulent flow needs to be resolved. The solution accuracy is governed by the number of cells in the domain. For a domain that measures 0.1 x 0.1 m the eddies may range from scales of 0.1 meter down to 10-100 micrometer. This makes it necessary to have meshes of 10^9 to 10^{12} nodes in order to resolve all eddies for methods such as DNS. DNS is a far more accurate way of calculating the flow but would be extremely computational intense for anything other than a very small domain. [15]

The fine mesh needed for the DNS-method is highly unrealistic with today's computers and thus time averaged turbulent schemes such as k- ε needs to be used. The k- ε model is the most widely used turbulence model and has been validated against a number of practical flows. It successfully predicts thin shear layers, boundary layers and duct flows without model adjustments for specific flows. It has been shown to perform extremely well where the Reynolds shear stresses are of importance in confined flows. It is however not as god at predicting unconfined flows, especially for weak shear layers, far-wake and mixing layers in separated flows. Further there are also some problems with large, rapid, extra strains such as highly curved boundary-layers or diverging passages. The main cause for these deficiencies is the assumption of an isotropic eddy viscosity. [15]

Large Eddy Simulation methods may be the future for predicting turbulent flows instead of today's two-equation models (k- ε, k-ω). LES requires more nodes and thus computational power and time to work which makes it of limited use today. [15]

Another common turbulence model is the k- ω model good near walls and for strong adverse pressure fields. It is however sensitive for the chosen ω value. [15]

The two-equation methods such as k- ε and k-ω build on time-averaged velocities. The instantaneous flow if split into one time averaged part and one fluctuating part according to equations 3.8 and 3.9 below. [16]

$$U = \bar{U} + u, \text{ Where } \bar{u} = 0 \tag{3.8}$$

$$\bar{U} = \frac{1}{2\Delta T}\int_{-t}^{t} U(\tau)d\tau \tag{3.9}$$

The turbulent k-equation, kinetic energy is defined according to equation 3.10 which then together with Navier-Stookes (N-S) and some further modeling assumptions as in equations 3.11-3.12. [15]

$$k = \frac{1}{2}\left(\overline{u^2} + \overline{v^2} + \overline{w^2}\right) = \frac{1}{2}\overline{u_\iota u_\iota} \tag{3.10}$$

$$P_k = \mu_t\left(\bar{U}_{i,j} + \bar{U}_{j,i}\right)\bar{U}_{i,j} - \frac{2}{3}\rho k \bar{U}_{i,i} \tag{3.11}$$

$$\left(\rho \bar{U}_j k\right)_{,j} = \left[\left(\mu + \frac{\mu_t}{\sigma_k}\right) k_{,j}\right]_{,j} + P_k - \rho\frac{k^{3/2}}{\ell} \tag{3.12}$$

The ε-equation is derived in a similar manner from N-S equation, where ε is defined as in equation 3.13. Combining with N-S equations and making some simplifications 3.14-3.17 can be obtained. [16]

$$\varepsilon = \frac{k^{3/2}}{\ell} \tag{3.13}$$

$$(\rho \bar{U}_j \varepsilon)_{,j} = \left[\left(\mu + \frac{\mu_t}{\sigma_\varepsilon}\right) \varepsilon_{,j}\right]_{,j} + \frac{\varepsilon}{k}(c_{\varepsilon 1}P_k - c_{\varepsilon 2}\rho\varepsilon) \tag{3.14}$$

$$P_k = \frac{P_\varepsilon}{c_{\varepsilon 1}\left(\frac{\varepsilon}{k}\right)} \tag{3.15}$$

$$P_\varepsilon = -c_{\varepsilon 1}\left(\frac{\varepsilon}{k}\right)\left(\overline{U}_{i,j} + \overline{U}_{j,i}\right)\overline{U}_{i,j} \tag{3.16}$$

$$dissipation\ term = -c_{\varepsilon 2}\rho\frac{\varepsilon^2}{k} \tag{3.17}$$

3.4. Computational Domain and meshing

The computational mesh is extremely important for the accuracy of the CFD-simulation. An ill-constructed mesh may yield poor results or may not even converge at all. Therefore there are many guide-lines to follow when constructing the computational mesh. Large aspect ratios and/or highly skewed cells should be avoided in the mesh. For high-order approximations it may be beneficial to first approximate a solution using lower-order schemes, this allows large imbalances to dissipate more quickly and adds an inherent stability to the numerical procedure. [15]

Further there exist several different types of cells used in CFD-meshes, the most common ones for volume meshing is hexagonal and tetrahedral cells. Tetrahedral cells are poor at resolving the boundary layer and may give rise to problems with diffusive fluxes. It is therefore common practice to use hexahedral elements close to boundaries and tetrahedral cells in the rest of the fluid domain. [15]

Cell aspect ratios (AR) should be kept between $0.2 < AR < 5$ in the interior fluid domain, it is however not as important at boundaries where $5 < AR$ may be necessary. The angle between gridlines should be kept close to 90degrees. If gridlines angle (se figure 9 and 10) are below 45° or above 135° numerical instabilities may arise and deterioration of the results can occur. [15] This is especially important near wall-, inlet- and outlet-boundaries. For triangular meshes ensure that the warp angle is below 75 degrees, see figure 10. Sudden changes in grid size should be avoided. These changes may otherwise destabilize numerical simulations by accumulation of truncation errors.

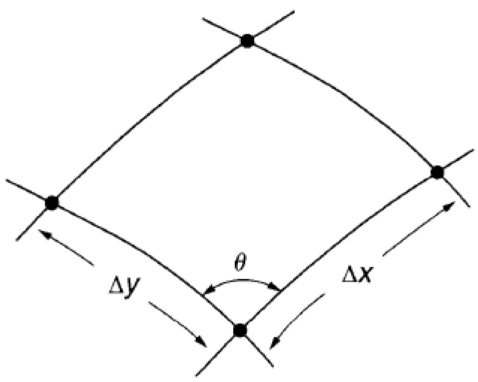

Figure 9: Sample of a grid with side's Δx and Δy and grid angle θ [15]

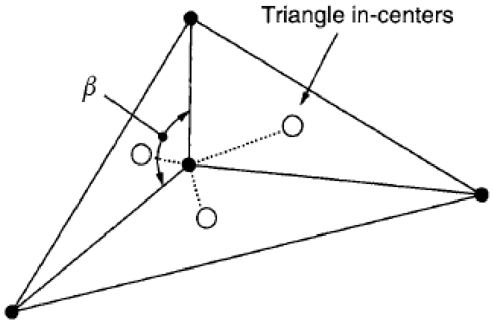

Figure 10: Sample of a tetra grid with a grid angle β [15]

3.4.1. Near wall meshing

Near the wall there is a boundary layer where the flow is decelerated down to zero velocity at the wall (no-slip condition). To capture the boundary layer effects of the flow the mesh used need to have a sufficiently high resolution close to the wall. When approaching the wall in a turbulent flow condition, the laminar viscous forces starts to dominate over the turbulent ones. This effect is gradual and makes it hard to predict the actual forces at some regions close to the wall.

The flow near the wall is usually divided into three groups shown in figure 11:

1. **Wall layer**: Flow dominated by viscous shear stresses.
2. **Overlap layer**: Both viscous and turbulent shear is important.
3. **Out region**: Turbulent shear stresses dominate the flow.

There is two common ways of imposing the wall boundary condition. One way is by resolving the wall boundary layer and the other way just the overlap layer is used by imposing so called wall functions. Since resolving the wall layer would require a very fine mesh and thus extensive simulation times the latter going to be used in this work.

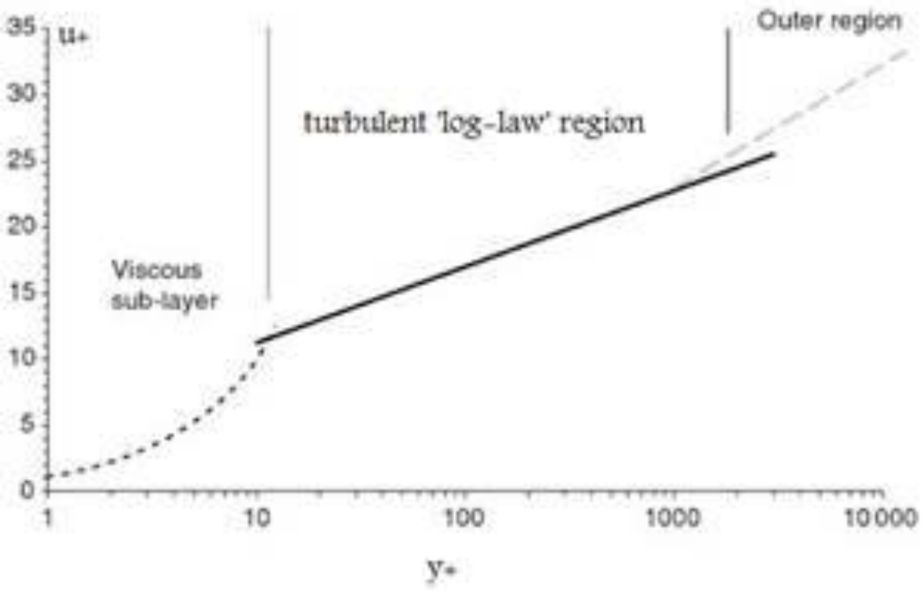

Figure 11: Log-law region illustration, [17]

In figure 11, the log-law and wall layer are shown. Where u^+ and y^+ are dimensionless properties defined in equation 3.18 and (3.19) below. [14]

$$u^+ = \frac{u}{u^*} = f\left(\frac{yu^*}{\nu}\right), \text{ where } u^* = \sqrt{\frac{\tau_w}{\rho}}, \tau_w = \mu\left(\frac{du}{dy}\right)_{y=0} \quad (3.18)$$

$$y^+ = \frac{yu^*}{\nu} \quad (3.19)$$

Where u is the local velocity parallel to the wall, y is the distance from the wall and τ_w is the wall shear stress.

For $y^+ < 5$ the wall layer applies which can be described according to equation 3.20.[14]

$$u^+ = \frac{u}{u^*} = \frac{yu^*}{\nu} = y^+ \quad (3.20)$$

Further out from the wall there is a region where both the wall layer and overlap layer influences the flow. This region should be avoided since there is no good way of describing the conditions in this layer. The overlap layer is sometimes also called the log-law and is valid for $30 < y^+ < 500$ [7]. It can be described by the relation in equation 3.21 below. [14]

$$u^+ = \frac{1}{\kappa}\ln(y^+) + B \quad (3.22)$$

Where the constants $B \approx 5.5$ and $\kappa \approx 0.4$ which are determined experimentally. They are valid universally for high Reynolds number turbulent flows past smooth walls [14].

Since u is not known at the node closest to the wall the distance y needs to be adjusted iteratively until y^+ is in the log-law region. The node is at the center of the computational cell and is used since all values calculated in the CFD code are averaged over the cell. Hence there is a condition at the resolution of the mesh close to the wall depending on the flow conditions.

CFX uses so called scalable wall-functions which is a reformulation of the standard wall function adapted to give an unique solution, making it possible to check for mesh independency by refining the mesh. It suggests putting at least 10 nodes into the boundary layer and that the upper limit for Y+ is 1000 if the Reynolds number is high (Re$\geq 10^9$) otherwise it is advisable to keep Y+ below 300. [18]

The scalable wall functions used by CFX is a different approach to eq. 3.19-3.22 to avoid singularities where $u^* \to 0, u^+ \to \infty$. Thus a reformulation is needed to avoid this as shown in equation 3.23-3.26. [18]

$$u^*_{CFX} = C_\mu^{1/4} k^{1/2} \quad (3.23)$$

$$u^* = \frac{u}{\frac{1}{\kappa}\ln(y^*) + C} \quad (3.24)$$

$$\tau_w = \rho u^*_{CFX} u^* \quad (3.25)$$

$$y^* = (\rho u^* \Delta y)/\mu \quad (3.26)$$

3.4.2. Guidelines for CFD-setup and sources of error

To obtain a good and accurate CFD-solution there are several guide-lines that should be followed. First off, it is recommended that transport variables like energy and scalar species is converged to 10^{-6} and 10^{-5} for scaled scalar species for quantitative convergence. [15]

There are several possible sources of errors in CFD simulations. These sources may be summarized as:

- Discretization error
- Round of error (truncation error)
- Iteration or convergence error
- Physical-modeling error
- Human error.

The first two are of high importance since they accumulate during the solution process. Reduced mesh or time-step size reduces the discretization error but instead increases the round of error. For really small sizes the effect is an increased total error since the computer only keeps a finite amount of decimals in its calculations. This can be avoided by not having many cells with small values, thus avoid round offs. [15]

To achieve fast convergence of the solution, a prescribed velocity profile at the inlet and a given pressure at the outlet are recommended. [15] Further a fluid may usually be assumed to be incompressible if the fluid flow velocity is well below the speed of sound in that fluid. [15]

4. Results and discussion

The model was setup and analyzed in several different steps. First, a steady state simulation with a simplified was run, and later a more complex model to determine the mesh-resolution needed as well as determining the stability of the simulations. By dividing the simulation into different steps it is easier to identify problematic areas as well as giving a better insight into what influences the pressure pulses.

Several different boundary conditions were tested and their impact evaluated. The turbulence model used in the subsequent simulations is the k-ε model. This model was chosen because of its strengths in confined flows and its accuracy for several different flows. Further the extensive validation of the model makes it a good choice for the simulations in this work.

The measure point in the hot leg (position 2 in figure 3) will not be included in the model; this is because it is far from the source of the pressure pulses. Further it is located close to the PRZ which is partially filled with steam which may a dampening effect.

4.1. Geometry and mesh

The geometry used in the simulations is a simplified model of the R2 reactor leaving out the core and main coolant loops. The model was constructed using ANSA. Further all dimensions used in the model are at room-temperature and thermal expansion is neglected. The thermal expansion of the system is assumed to be small compared to the size of the domain.

Two different models was constructed, the first one is a heavily simplified model consisting of only the main geometrical features of the system, se figure 12. This first model is used for the first transient simulations where the motion is checked and the behavior of the pressure pulses for different core barrel displacements are evaluated. The second model is a more detailed model where more features of the core barrel and primary inlets have been added, see figure 13. These additions should be able to give a more accurate prediction of the flow than the first simplified model.

The mesh for the second model was refined in several steps. Layers of thin cells close to the walls were added in an attempt to resolve the boundary layer but later skipped due to convergence problems. Normally the growth rate of the cell thickness should be kept at or below 1.2 but since the geometry in question is large it is not feasible due to limitations in computational resources. Following this growth rate would result in more than 35-40 layers at some places and since the surface mesh consists of about 350 000 cells, this would result in 14 million cells just for the layers close to the wall. This is not practical given the computational recourses available for this work. Several meshes where tried, first with a thin layer of 3-9 cells with a large change in cell size to the bulk cells. Several iterations of 9 layers with slightly larger growth rates where tried to minimize the gap in size to the bulk cells. Neither of these approached gave a stable system. Mesh-layers were therefore not used in the simulation meshes resulting in un-resolved boundary layers.

The quality of each mesh where checked with Ansa:s built in “Mesh Quality” feature where the mesh was checked against skewed and other bad quality cells. Parts of the mesh for the full model can be seen in figure 14 and 15.

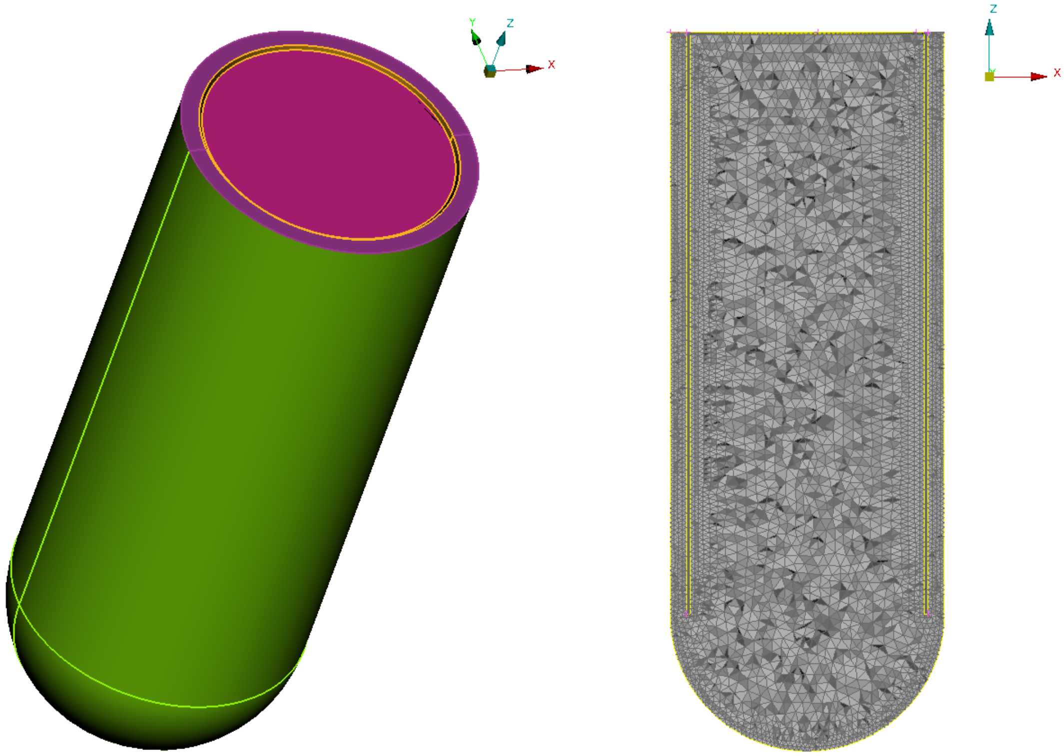

Figure 12: First simplified model

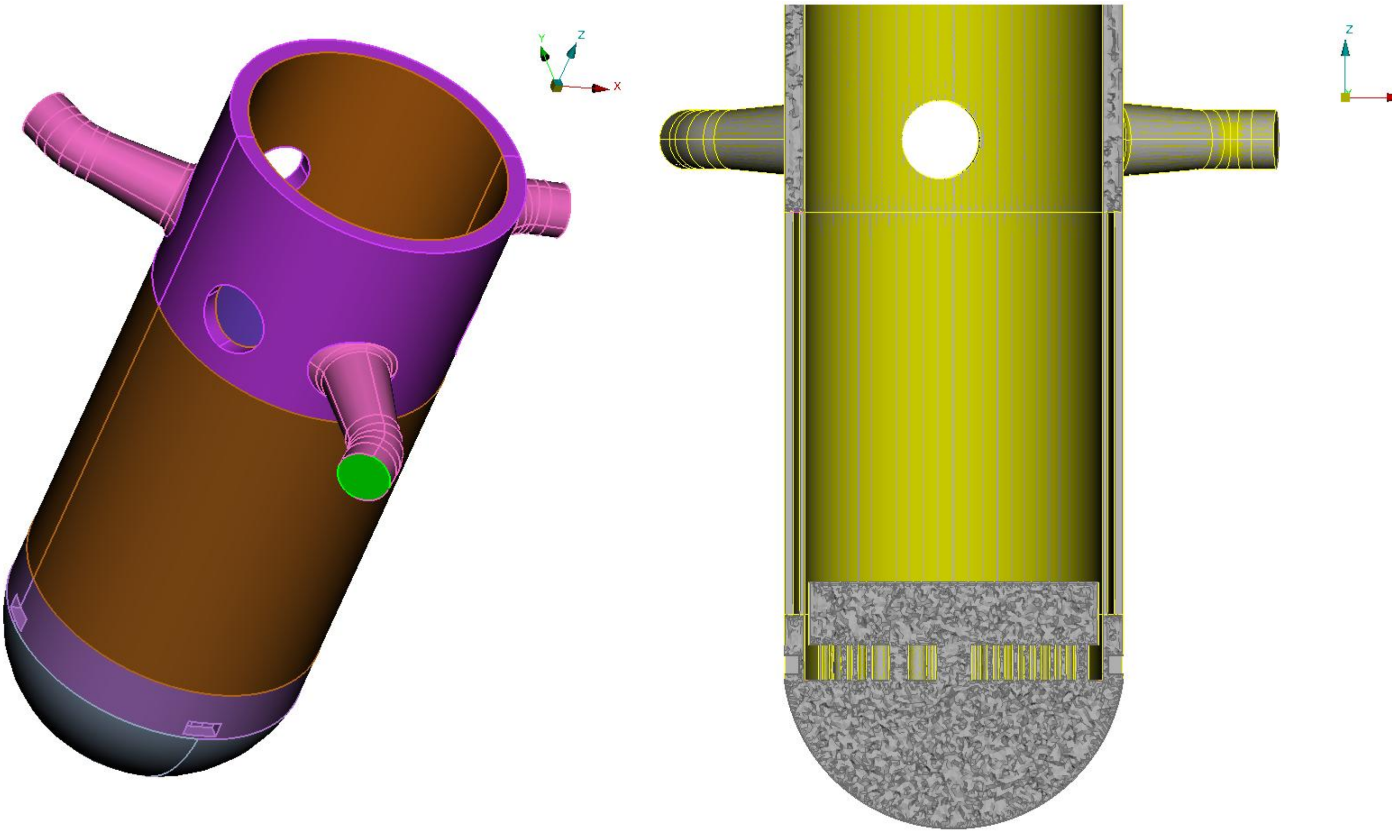

Figure 13: Second full model for more accurate flow prediction

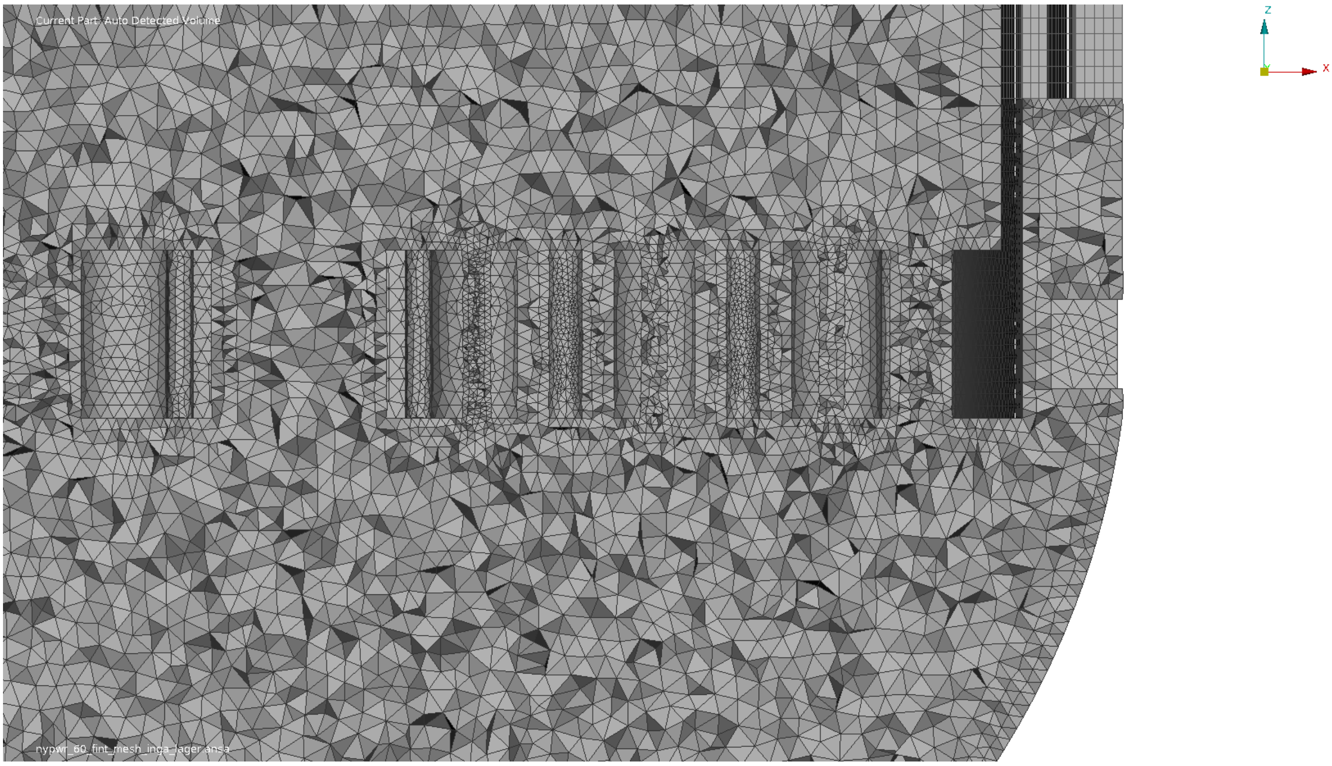

Figure 14: Zoomed in view of the second full model

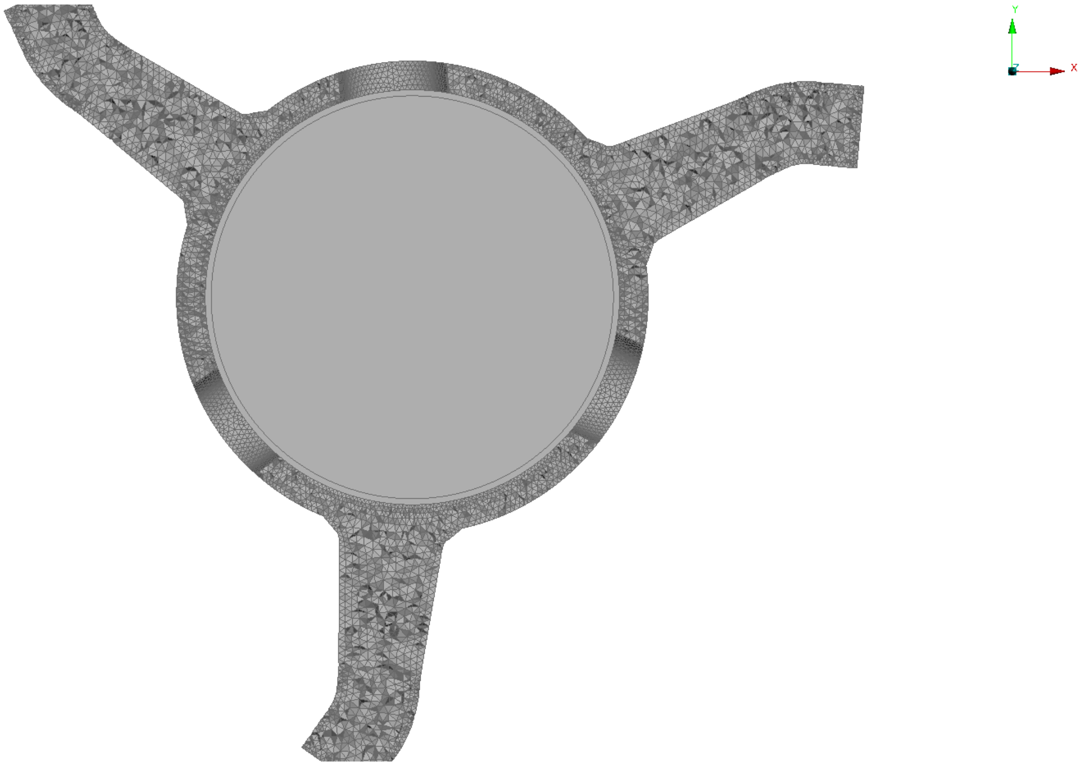

Figure 15: Overview of cells in second full model

4.2. Boundary conditions and assumptions

To be able to determine the boundary conditions best describing the flow in the reactor as well as determining the needed mesh resolution several steady state simulations were performed on both models. For these simulations all walls are considered stationary and the effect of the guide tubes on the flow is neglected.

The inlet boundary condition is set to a mass flow boundary condition. By specifying the inlet mass flow CFX will adjust the pressure accordingly, giving the desired mass flow into the domain. The mean inlet mass flow over all the three inlets (Inlet 1-3) is known. The mass flow is assumed to be equally divided between all three inlets. The inlet mass flow is listed in table 3, resulting in a mass flow of $4582.33\,kg/s$ at each inlet. For the later transient simulations both pressure and mass flow inlets where tested on the simplified model. The effect on these boundary conditions will be discussed in more detail when describing the transient simulations.

The major simplification in both the models is the outlet boundary condition, where the domain is cut of just before the reactor core. This is done to avoid resolving the core and the upper plenum, saving large amounts of cells and thus computational time as well as avoiding heat transfer in the simulation. The location of the boundary condition is not optimal since it is in the middle of the flow domain of the reactor. However the placement of the outlet is a tradeoff between accuracy and complexity of the system. Since the system is very large this trade-off needs to done to keep the computational resources required at a manageable level, see figure 13.

In the first simplified model backflow at the outlet is avoided by extending the outlet sufficiently, this is possible due to the low mesh-resolution used for this model. For the full model a steady state simulation was run with an “outlet” boundary condition; this simulation showed that there would be some backflow into the domain. A second simulation showed that by including the lower core plate removed all the backflow and resulted in a more stable and faster converging system. Thus in subsequent simulations on the full model the lower core plate will be included in all simulations with an ordinary pressure outlet boundary condition for both models.

Since the domain is cut before the core some additional pressure drops needs to be estimated to determine the outlet pressure of the domain. The pressure known is measured in the pressurizer (PRZ) as 15.51 MPa. The PRZ is located 11 meters above the main coolant loops, giving an additional 0.08 MPa in pressure in the hot leg due to gravitational effects; this can be seen in equation 4.1.

$$p_{loop} = p_{PRZ} + \rho g h \approx 15.59\ MPa \tag{4.1}$$

Further the pressure drop over the core and core plates for the core design in question is assumed to be according to equation 4.2. [19]

$$\Delta p_{core} \approx -0.18\ MPa \tag{4.2}$$

The pressure drop between the upper plenum and the primary coolant loops is assumed to be according to equation 4.3. [19]

$$\Delta p_{HT} = -0.1\ MPa \tag{4.3}$$

$$p_{outlet} = p_{loop} - \Delta p_{HT} - \Delta p_{PRZ} \approx 15{,}87\ MPa \tag{4.4}$$

Summing the pressure drops (see equation 4.4) yields an outlet pressure of 15.87 MPa. Since the inlet boundary condition is set as a mass flow inlet, the actual outlet pressure does not influence the solution to any larger degree. The inlet pressure is adjusted to give a certain mass flow in the inlets given the outlet pressure. Since the fluid properties are set according to a set pressure the only difference the actual outlet pressure makes is the addition of the same pressure to every point in the flow. The fluid properties are only slightly affected by a change in pressure of the magnitude in question and thus the solution should not be affected much by these assumptions.

The walls of the reactor core are modeled as adiabatic walls with a no-slip condition. It is assumed that the reactor has been running at constant and full power for sufficiently long time for a steady state condition to be achieved and that all materials making up the reactor has been heated up. In that state it is further assumed that the heat flow through the walls is negligible compared to the energy content carried by the coolant, thus an adiabatic boundary condition is used. The walls are assumed to be smooth with a no-slip condition. In table 3 below the main input data used for the model and the boundary conditions can be seen.

Table 3: Boundary conditions used

Boundary:	Condition:	Value
Inlet	Mass flow/Pressure in	$\dot{m} = 13747\ {}^{kg}/_{s}$ $T_{in} = 287\ ℃$
Walls	Adiabatic, smooth, no-slip	-
Outlet	Pressure outlet	$p_{outlet} \approx 15{,}87\ MPa$

Further all simulations performed were done with 2^{nd}- order accurate schemes unless otherwise is specified. The schemes in question are Ansys ® CFX proprietary schemes called “High Resolution”. Since the pressure fluctuation are small compared to the actual system pressure a reference pressure of 15.0 MPa is used. The reference pressure together with the option “Double precision” is used in all simulations to minimize round of errors in the calculations.

4.2.1. Transient treatment

For the transient simulations a scheme called “Second order backwards Euler” were used in which is a second order accurate scheme. The transient is started at time $t = 0\ s$ from a converged steady-state solution. There was however a small jump in pressures at the measuring points at the start of the transient. This is probably due to the description of the motion. Since the motion is described by a since-wave, at time 0 the derivative is very large. The large derivative makes the acceleration of the core barrel large in the first time-steps of the transient. This is however remedied when the quasi-stable solution is obtained by running the transient simulation for several core barrel motion periods.

For the transient simulations, a time-step and total simulation time needs to be chosen. The choice of a time-step is based on the dimensionless Courant number. The Courant number describes the time it takes for one fluid particle to travel trough the smallest cell in the mesh. A time-step should be small enough so that a fluid particle never has the time to travel through more than one cell, to avoid loss of information. The courant number for one dimension is defined in equation 4.10 below and should be kept as low as possible. For an explicit scheme it is important to keep the courant number below one but for implicit schemes it is usually sufficient to keep it below ten. [18]

$$Co \equiv \frac{u\Delta t}{\Delta x} \approx 1 \qquad (4.10)$$

For the simplified geometry with 1.3 million cells the Courant number was about 1.2 with a time-step of $\Delta t = 0.01$ s and 1.8 with the 4 million cells full model case $\Delta t = 0.005$ s.

Further it is important that one fluid particle has time to flow through the whole domain during the transient time to be able to reach a quasi-steady state. Thus the total simulation time can be estimated using the mean fluid velocity and the length of the fluid path.

Using the first transient simulation with 1.3 million cells as an example, we have a mean fluid velocity of about 5 $\mathrm{m/s}$ and an average fluid path of 22 m. This would give a total transient time of about 4.4 s giving the condition stated above. In the case of the more complex model used in this work, the fluid path is about 13 m, giving a needed transient simulation time of about 2.6 s to reach quasi-steady-state.

Further the motion or rate of change in the transient needs to be sufficiently resolved, in this case the 7.2 Hz sinusoidal vibration. The time-step needs to be sufficiently small to capture all the features of the vibration. With the time-steps of $\Delta t = 0.01$ s and the $\Delta t = 0.005$ s the sinus motion is captured 14 and 28 times respectively each period which is captures the motion well.

4.3.1 Coolant properties

In table 4 below the coolant properties used are shown. The physical properties of the coolant are assumed to that of water at the temperature and pressure in question. Although the coolant contains some additives of boron, the effect on the physical properties of the coolant is assumed to be negligible. It is assumed that no significant heat transfer to the coolant is present before the reactor core, thus the coolant temperature is assumed to be about 287 ℃. Given the outlet pressure later simulations will show of an average coolant pressure of about $15{,}9\ MPa$ which is used for the coolant reference state.

Table 4: Physical properties of water, [20]

Physical properties for water at 287 ℃ and 15.9 MPa		
M	$18.0153\ {}^{g}/_{mol}$	Molar mass
μ	$93.7 * 10^{-6}\ Pa * s$	Dynamic viscosity
$\rho_{@287°C}$	$752.4 \frac{kg}{m^3}$	Density
c_p	$5180\ {}^{J}/_{kg\ K}$	Specific heat capacity
β	0.00243 1/K	Thermal expansion coefficient
k	0.586 W/(m K)	Thermal conductivity

4.3. Mesh deformation

The motion of the core barrel is handled via CFX: s mesh deformation function, where the boundaries are moved by deforming the mesh. As stated earlier the motion of the core barrel will be assumed to be a simple pendulum motion with the amplitude of 1 mm and frequency of 7.2 Hz. The frequency used is the lowest Eigen-mode of the core barrel determined from independent structural calculations and is only used as an assumption in this work.

The motion is achieved by referring the boundaries and nodes in the mesh via a cylindrical coordinate system. The cylindrical coordinate system is defined as in figure 16. The theta component of the system is expressed as an arc length. The arc length, denoted S is defined according to equation 4.5 below where r the radius and θ the angle of the coordinate system.

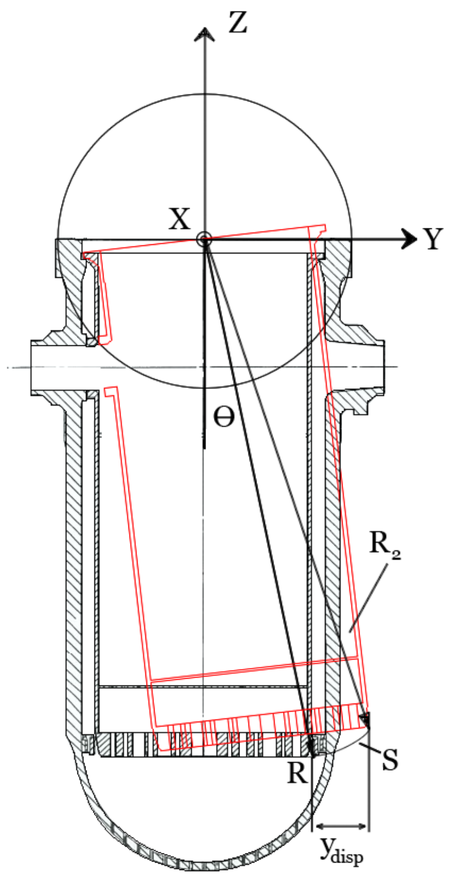

Figure 16: Core barrel displacement expressed in a cylindrical coordinate system

$$S = r\theta \tag{4.5}$$

The radius r is the distance from each node in the mesh. This distance can be described by using Pythagoras theorem in equation 4.6 where y and z are the Cartesian coordinates for each node with the same origin as the cylindrical system.

$$r = \sqrt{y^2 + z^2} \tag{4.6}$$

The amplitude of the displacement also needs to be expressed in this new coordinate system, this is done using simple trigonometry, expressing a hypothetical point in the bottom part of the core barrel and solve for the angle θ corresponding to that displacement as seen in equation 4.7 with angles according to figure 17.

$$\begin{cases} \theta_{max} = \sin^{-1}(\frac{y_{barrel}}{r_{max}}) \\ \alpha = \frac{\pi}{2} - \cos^{-1}(\theta_{max}) \\ \theta = \sin^{-1}\left(\frac{y_{disp}}{r_{max}\cos\alpha}\right) \end{cases} \tag{4.7}$$

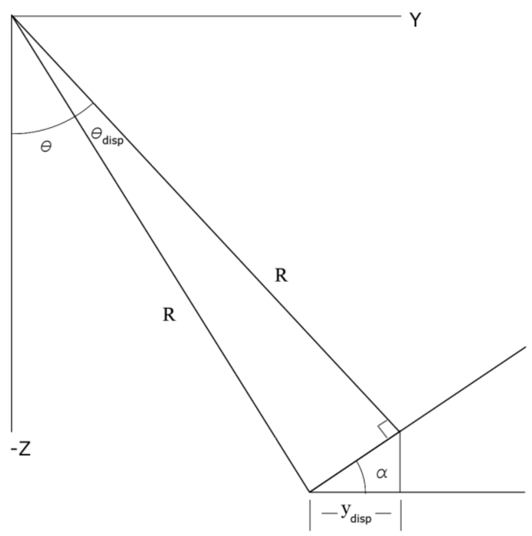

Figure 17: y-displacement and angle definitions

Knowing the maximum displacement angle θ it is just a matter of applying the sinusoidal pendulum movement, this is implemented according to equation 4.8 below where t is the time and f is the frequency of the core barrel motion.

$$\sin(2\pi tf) \tag{4.8}$$

Combining equations 4.5-4.8 then gives the expression for the arc-length as a function of time, see equation 4.9. This expression is then used in CFX to describe to movement as a displacement. In figure 18 the corresponding arc-length as calculated by equation 4.9 is plotted versus time.

$$S = \sqrt{y^2 + z^2}\,\sin(2\pi tf)\,\sin^{-1}\left(\frac{y_{disp}}{r_{max}\cos\alpha}\right) \tag{4.9}$$

Figure 19 shows an exaggerated core barrel displacement from a test simulation where the fluid flow equations where disabled and only the mesh deformation solved.

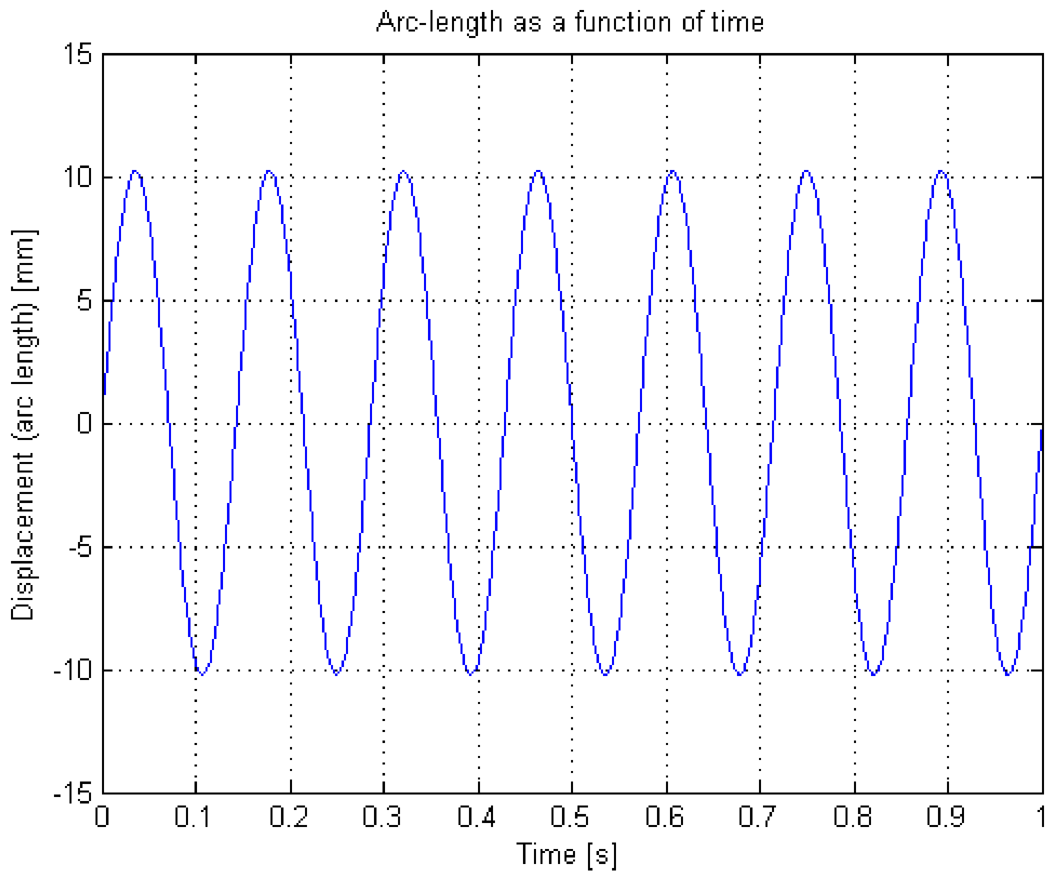

Figure 18: Core barrel displacement expressed as an arc-length

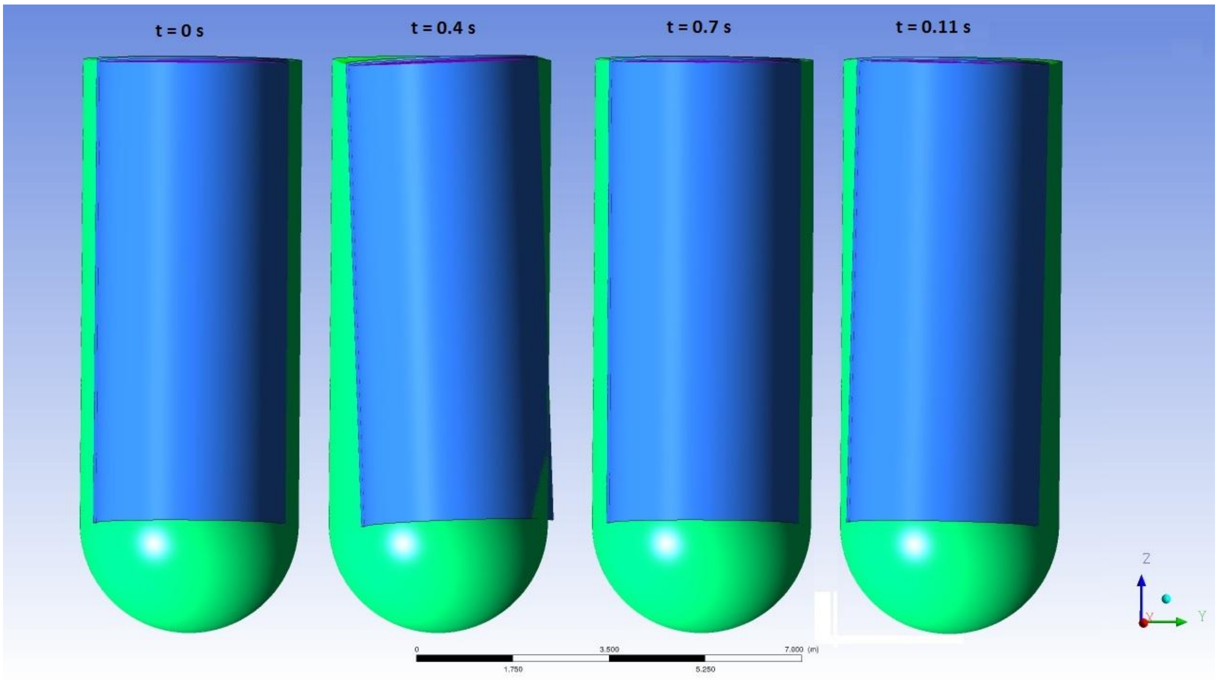

Figure 19: Core barrel movement at different times

4.4. Simulation results

In this subchapter the result from the different simulations will be presented. Several different simulations where performed on the two different models, the results from which will be presented and put into context. A generalized CFX input file for all the simulations can be found in appendix A. Further tabulated amplitude data for all simulations can be found in appendix B and detailed plots of the pressure versus time for the different simulations can be found in appendix C.

The focus is directed upon the pressure variations in the different guide-tubes available for measurements. These guide tubes are referred to using a coordinate system R-A and 1-15 for the different tube positions. This is illustrated in figure 20 below where the available guide tubes have been marked. Further the coordinate system used in the simulations can be seen in the lower right corner of figure 20. Hence forth all locations will be referred to either by the reactor coordinate system of the Cartesian coordinate system.

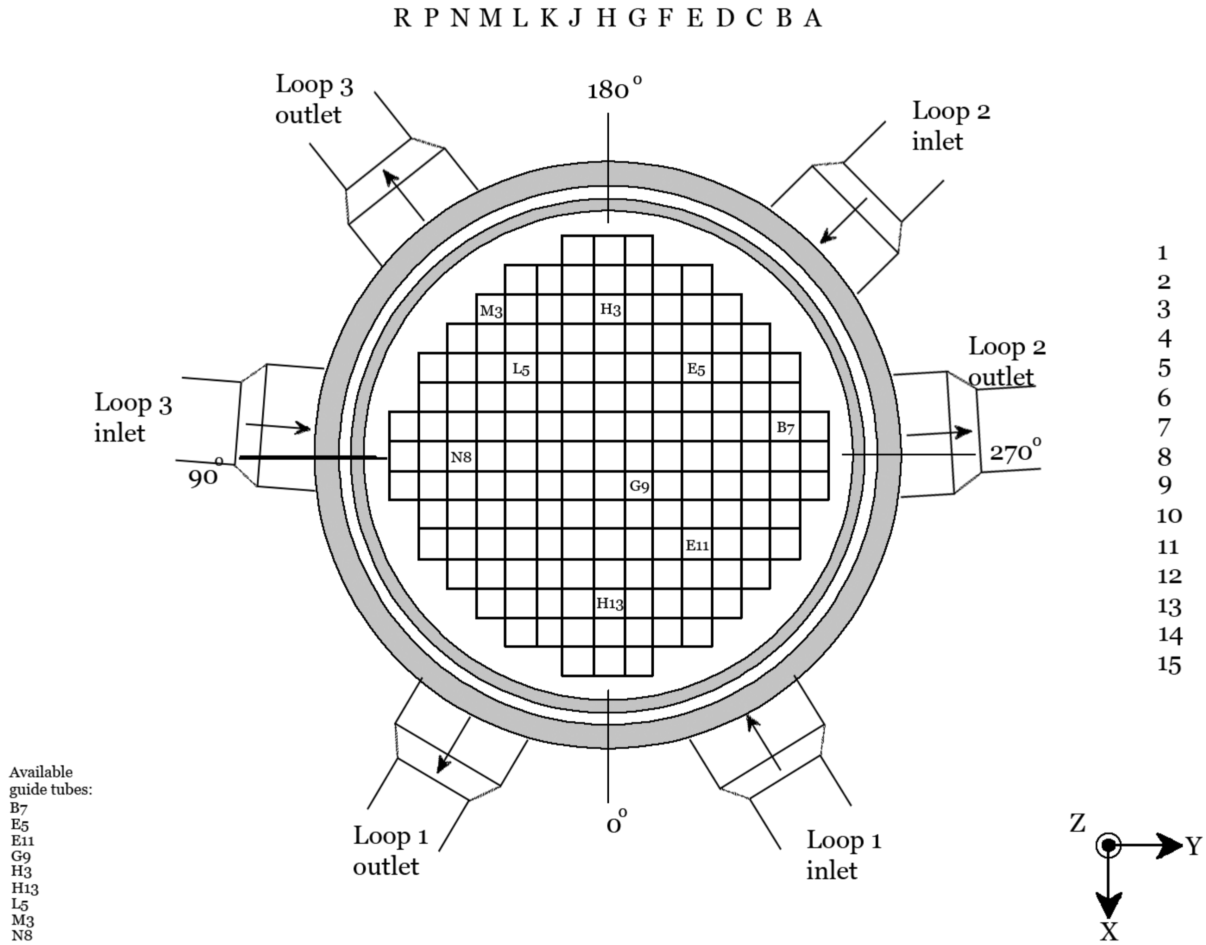

Figure 20: Reactor core coordinate system

The simulations to be performed with corresponding boundary conditions, mesh used and simulation type is presented in table 5 below. For all simulations the walls are adiabatic with no-slip and heat transfer is neglected. The direction of motion is referring to direction of the pendulum motion and is relative the X-Y coordinate system shown in the lower right corner of figure 20.

Table 5: Simulation overview with corresponding boundary conditions and motion type for the simulations performed

Mesh:	Type:	Inlet boundary condition	Displacement	Frequency	Direction	Time-step
Simplified model	Steady state	Mass flow	N/A	N/A	N/A	N/A
	Transient	Pressure inlet	1, 5, 10 mm	7.2 Hz /	Y-direction	0.01 s
		Mass flow	0.5, 1, 2.5, 5, 10, 15 mm	7.2 Hz /	Y-direction	0.01 s
			1 mm	7.2 Hz /	X-direction	0.01 s
Full model	Steady state	Mass flow	N/A	N/A	N/A	N/A
	Transient	Mass flow	1 mm	7.2 Hz /	Y-direction	0.005 s
			1 mm	7.2 Hz /	Y-direction	0.0025 s

Simplified model

Several simulations with different core barrel displacements, motion direction and boundary conditions were performed on the simplified model. The main findings will be presented here.

For transient simulations a steady state simulation is needed initiate the transient. Therefore a steady state simulation was performed on the simplified model. The steady state simulation showed of an unexpected flow behavior with only one symmetry plane instead of two as would be expected. The results have been checked against two different meshes, the first with 1.3 million cells and a second mesh with about 3 million cells. These results are thus mesh-independent. The steady-state solution shows that two vortices appear se figure 21. This is not the flow situation in the full model used in later simulations where only one vortex is formed. The flow behavior in the first series of simulations is however not as important and should be regarded as a proof of concept. These simulations are performed to get the general behavior if the pressure inside a moving system.

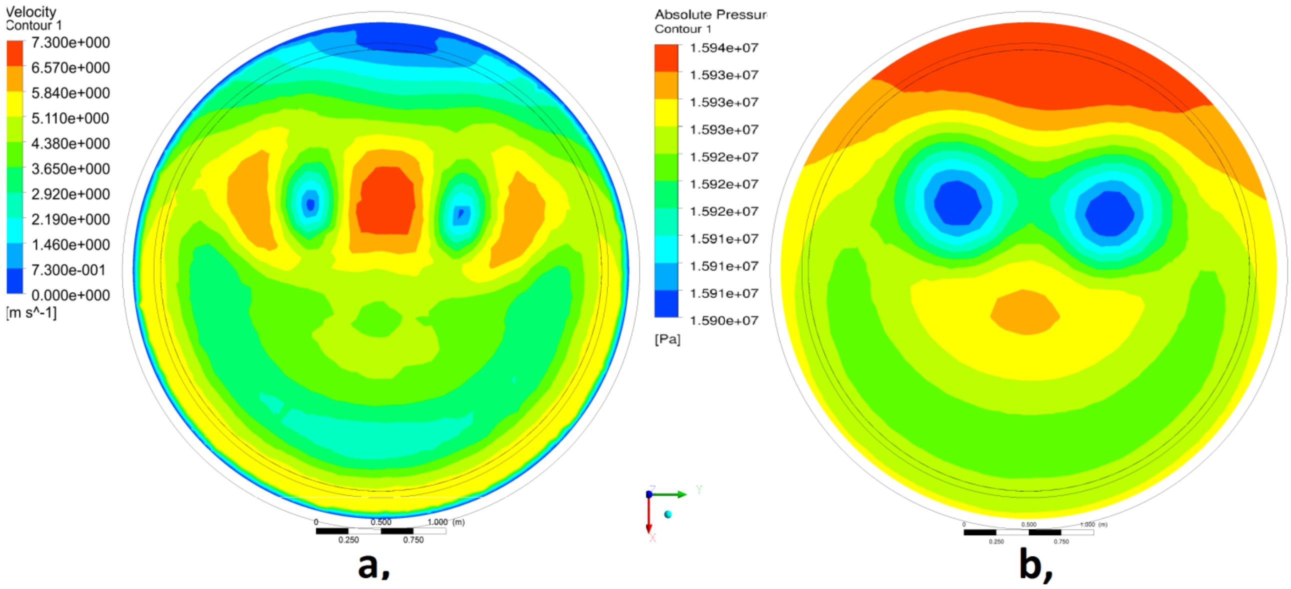

Figure 21: a, Velocity for simplified model at bottom of the core barrel, b, Absolute pressure for guide tube plane in the simplified model

The following transient simulations were started from the converged steady state simulations discussed earlier. The courant number was about 1.2 and quasi-steady state condition was achieved after transient time of about 3-6 seconds.

The first simulation was with a 10mm displacement and a mass flow inlet boundary condition. The highest amplitudes can be observed at the positions for tube B7 and N8 with a peak to peak amplitude of 0.009 and 0.008 MPa respectively. Thus it seems like the tubes closest to the periphery is subjected to the largest pressure fluctuations, see figure 22. In the figure, available guide tubes are circled in red. Further the available guide tube closest to the middle shows the lowest fluctuation, which supports the theory of higher amplitudes further out. In this simulation the inlet boundary condition is set as a mass flow inlet. The average inlet pressure over all three inlets can be seen in figure 23 as the circle-bullets.

From the figure it can be seen that the inlet pressure varies with different amplitude and does not show the sinus shape as the other measurement points. To be certain this fluctuation is not the cause for the observed pulsations in the guide tubes positions another simulation with a pressure inlet boundary conditions was performed. This simulation showed similar results, with almost identical fluctuations in all tubes. The flow was about 6% smaller with the pressure inlet which may explain a very slight reduction in amplitude.

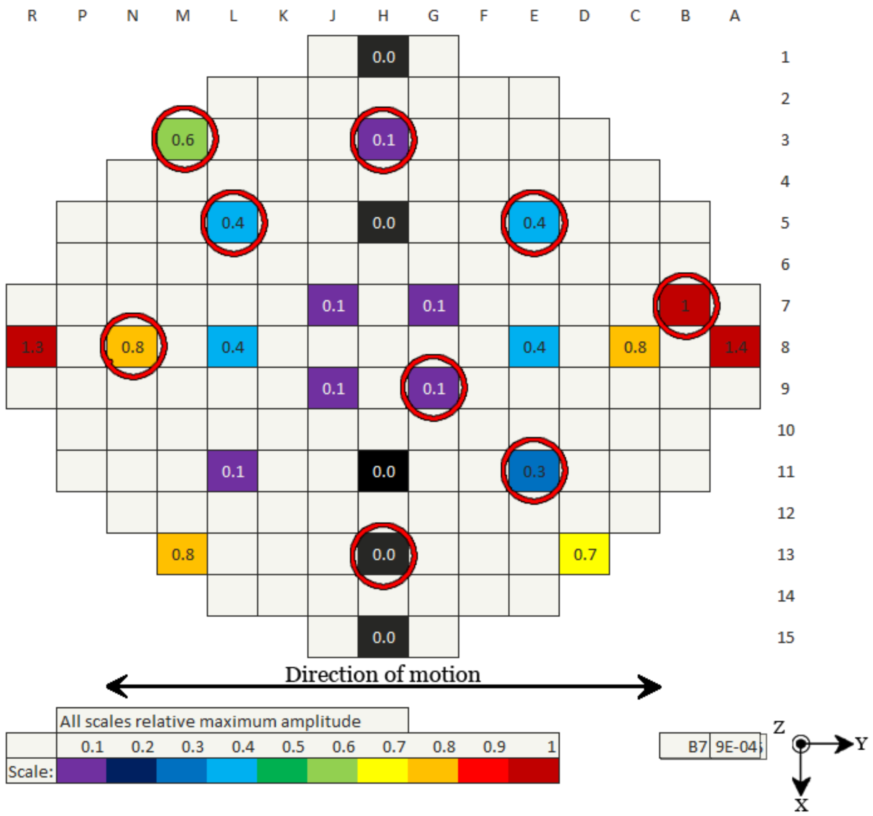

Figure 22: Pressure amplitude at the different guide tubes, relative guide tube B7. Simplified model, 10mm displacement and Mass inlet, tubes available for measurements are circled in red

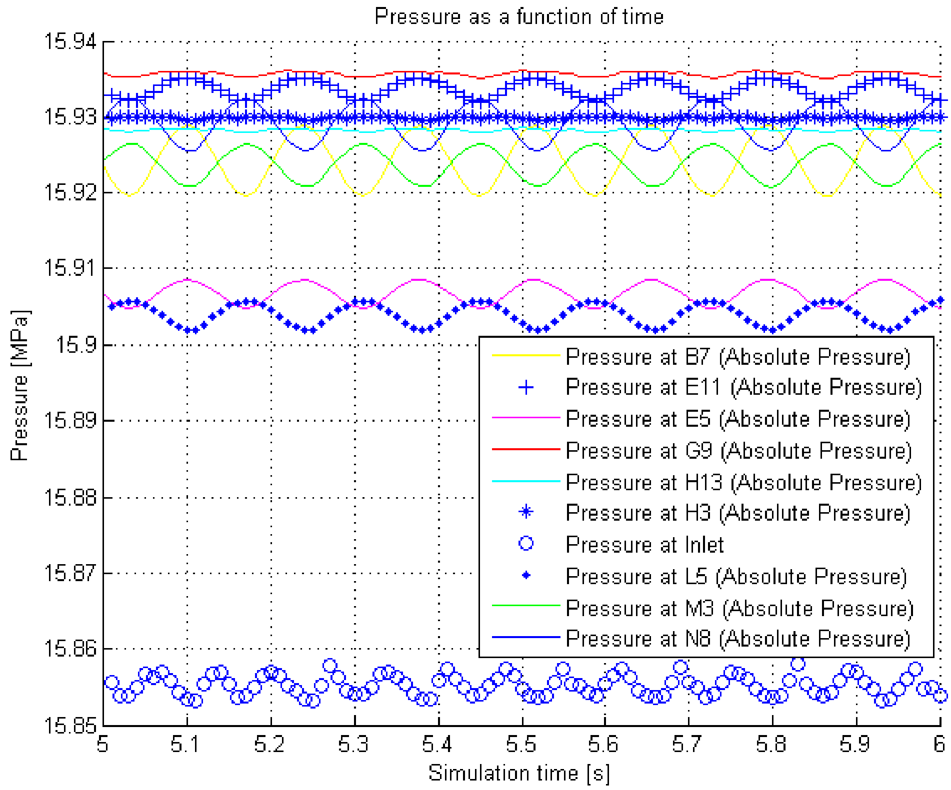

Figure 23: Pressure versus time for the simplified model with 10mm displacement and mass flow inlet

Several simulations with core barrel displacement of 0.5, 1, 2.5, 5, 10 and 15 mm where performed to determine the relation between the amplitude of the pressure pulsations and the core barrel displacement. The pressure fluctuations for the 1mm case are presented in figures 24 and 25.

From figure 25 it is clear that the amplitude of the different pressure variations is much smaller than for the 10mm displacement. There is however still possible to discern a sinus-shaped pressure variation at several of the guide tube-position. As in the two previous simulations the amplitude of the pressure response is largest at tube B7, in this simulation the peak-to-peak amplitude is about 0.0009 MPa. The amplitude of all the measurements points is reduced with about a factor 10 from the previous simulation suggesting a linear relation to core barrel displacement.

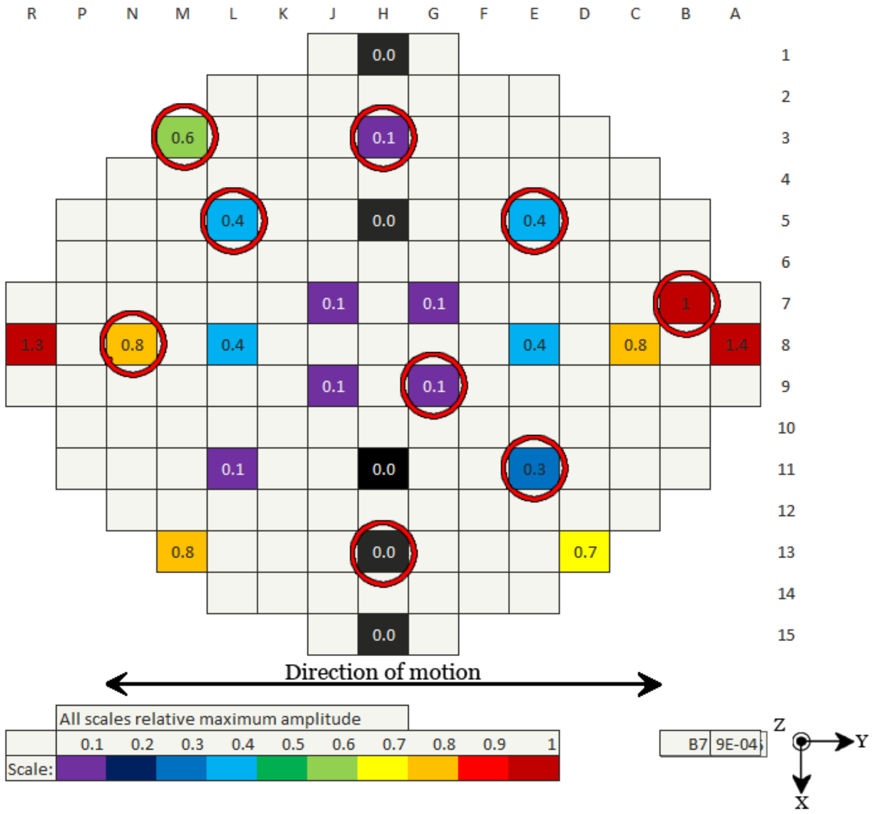

Figure 24: Relative pressure amplitude at the different guide tubes, relative guide tube B7. Simplified model, 1mm displacement and mass flow inlet, tubes available for measurements are circled in red

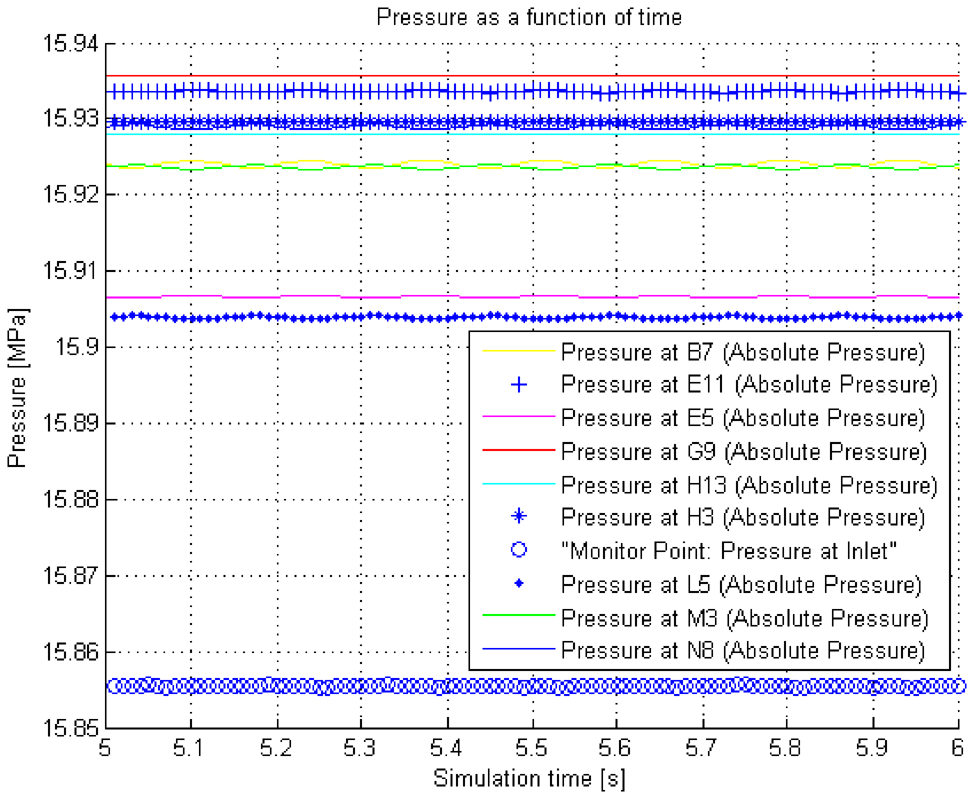

Figure 25: Pressure versus time for simplified model with 1mm displacement and mass flow inlet

To further investigate the relation between the pressure pulses and core barrel displacement, figure 26 shows the pressure in guide tube B7 versus time for several different core barrel displacements 1, 5 and 10mm with the mass inlet boundary condition. Further the amplitude of the pressure pulses versus core barrel displacement can be seen in figure 27. From the points simulated the pressure amplitude response to the core barrel displacement seems to be almost linear.

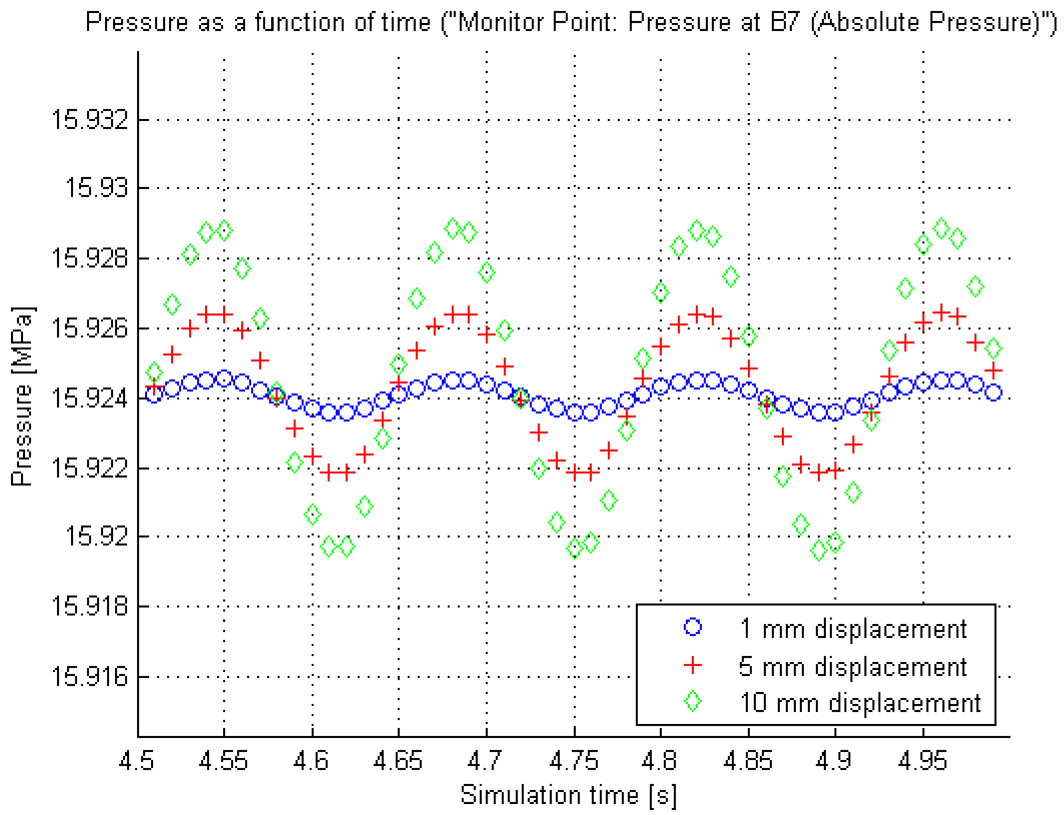

Figure 26: Pressure in guide tube B7 versus time for different core barrel displacements on the simplified model (mass flow inlet)

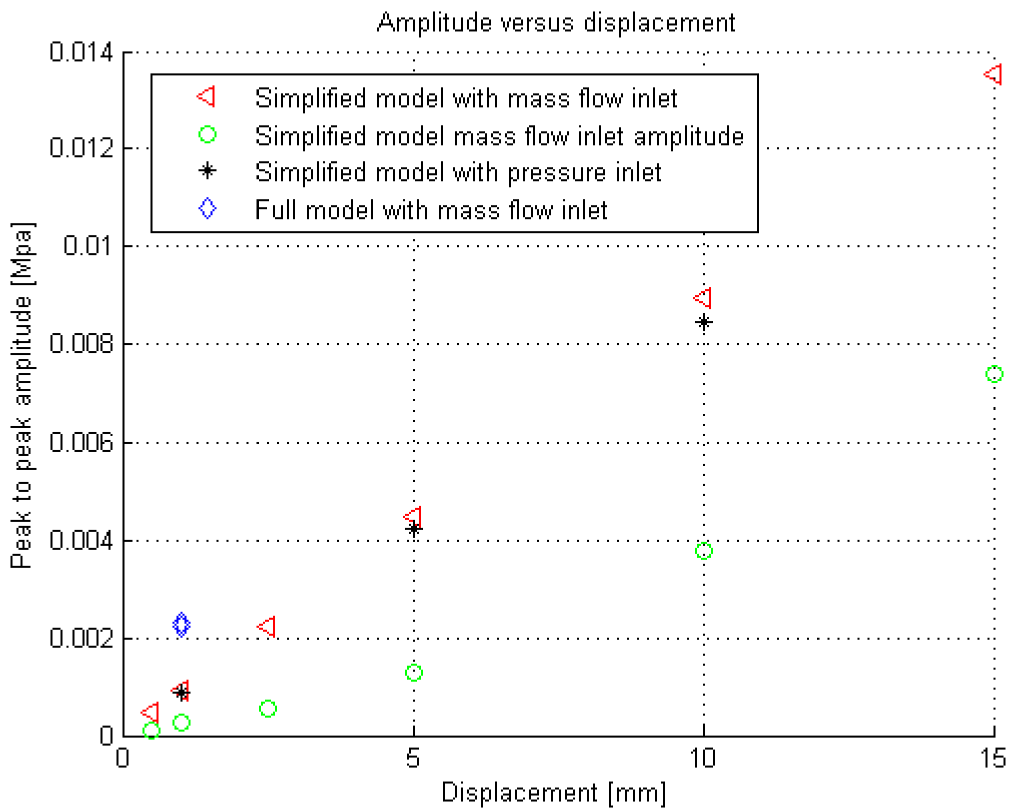

Figure 27: Pressure amplitude versus core barrel displacement on the simplified model

Finally a simulation where the motion of the core barrel is about the y-axis (see figure 20) resulting in a perpendicular motion to the previous one. The amplitude map from this simulation is presented in figure 28 below. From this figure it is possible to observe the same behavior as the previous simulations with the highest amplitudes closest to the motion apexes. This would imply that the pulses observed are more influenced by the direction of the motion than the orientation of the flow.

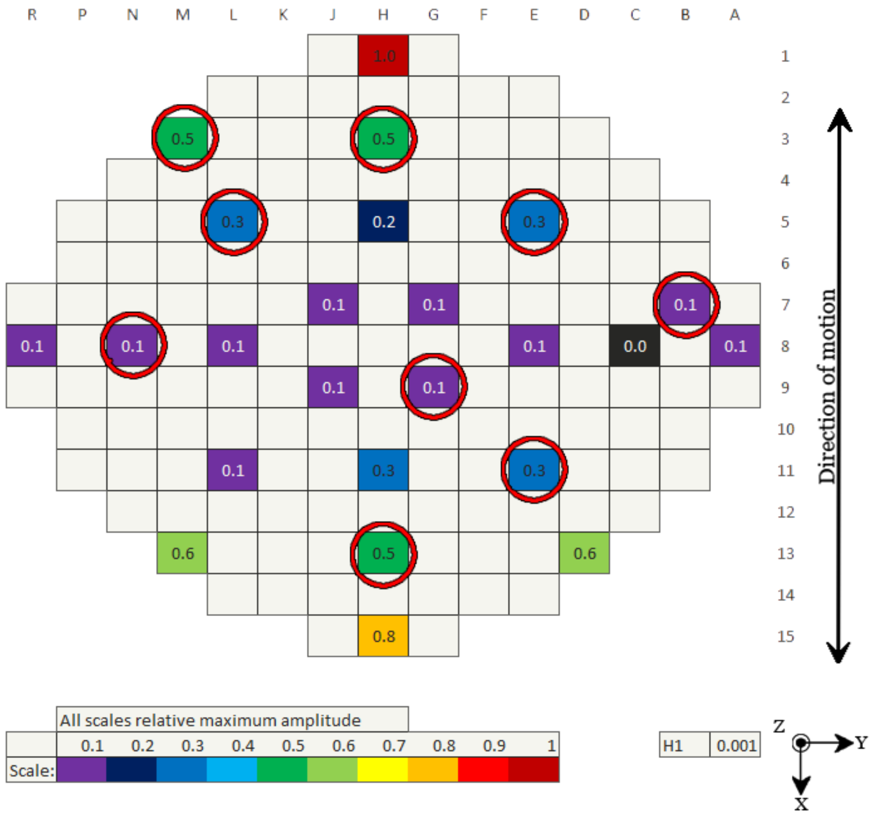

Figure 28: Relative pressure amplitude at the different guide tubes, relative guide tube B7. Simplified model, 1mm displacement, around y and mass flow inlet, tubes available for measurements are circled in red

Full model

Since there was no substantial effect of the mass flow inlet compared to the pressure inlet boundary conditions on the simplified model the first one is used for all simulations with the full model. The mass flow inlet boundary condition is chosen since it results in a more stable system. Further the influence of the inlet boundary should be less pronounced in this model since the inlet is further from the points of interest.

The full model was simulated with successively finer meshes. Starting out with a 2 million cells mesh. Due to computer limitation the final mesh is only 4 million cells. For larger meshes the computer memory is insufficient making the calculations extremely slow. This makes it hard to check if the solution is mesh independent. There is only small differences between the 2 million mesh solution and the 4 million one.

The solutions were compared with the pressure at the guide tube positions, maximum and minimum velocities, maximum and minimum pressure and wall shear stress. The largest difference can be found for the average wall shear stress which experienced a 20 % increase. Since the boundary layer is not resolved it would be hard to get a mesh independent solution. The differences of the pressure at the different locations monitored were all less than 0.1 %.

The solution converged after about 3000 iterations. From the full model the flow looks a bit differently from the simplified model used in simulations 1-4. This is mainly because of the three inlets with their 30° inlet angle. This gives the flow a rotation around the z-axis, see figure 29. The rotation creates a small vortex in the bottom of the RPV stabilizing the flow and distributes the coolant from the different loops more evenly than for the simplified model. The perforated core barrel bottom counteracts this rotation and directs the flow into a more upward direction while the lower core barrel plate distributes the flow evenly, see figure 30.

Looking at the pressure it can be seen from figure 31 to 32 that the highest pressure is found in the down comer close to the periphery. The pressure is at its highest at the core barrel wall in front of the inlets. A lower pressure area can be found close to the center inside the flow vortex. More detailed figures of the flow behavior in the system can be found in appendix D.

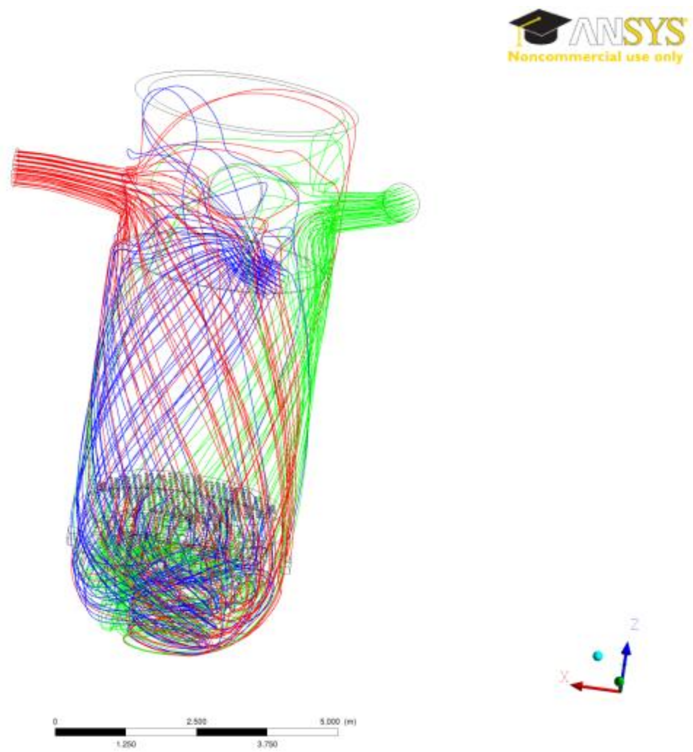

Figure 29: Stream lines colored by inlet, (red, green and blue for inlets 1, 2 and 3 respectively) for the full model

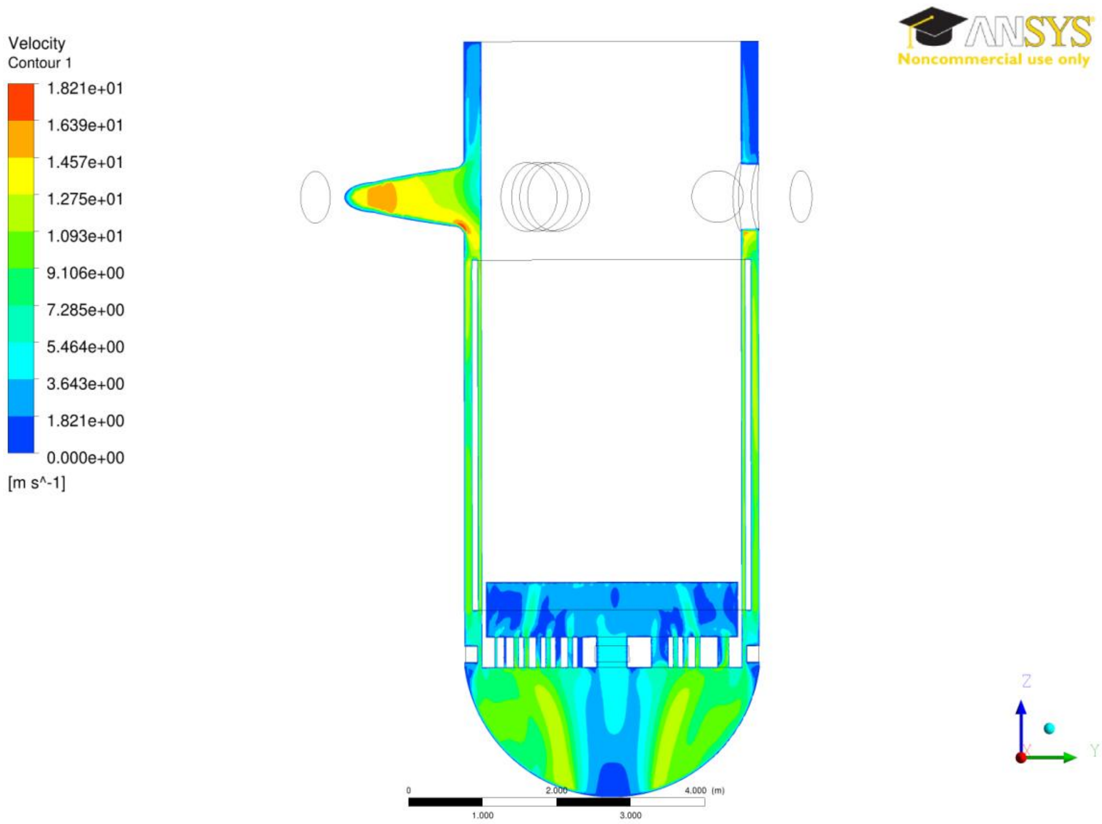

Figure 30: Velocity in the YZ-plane

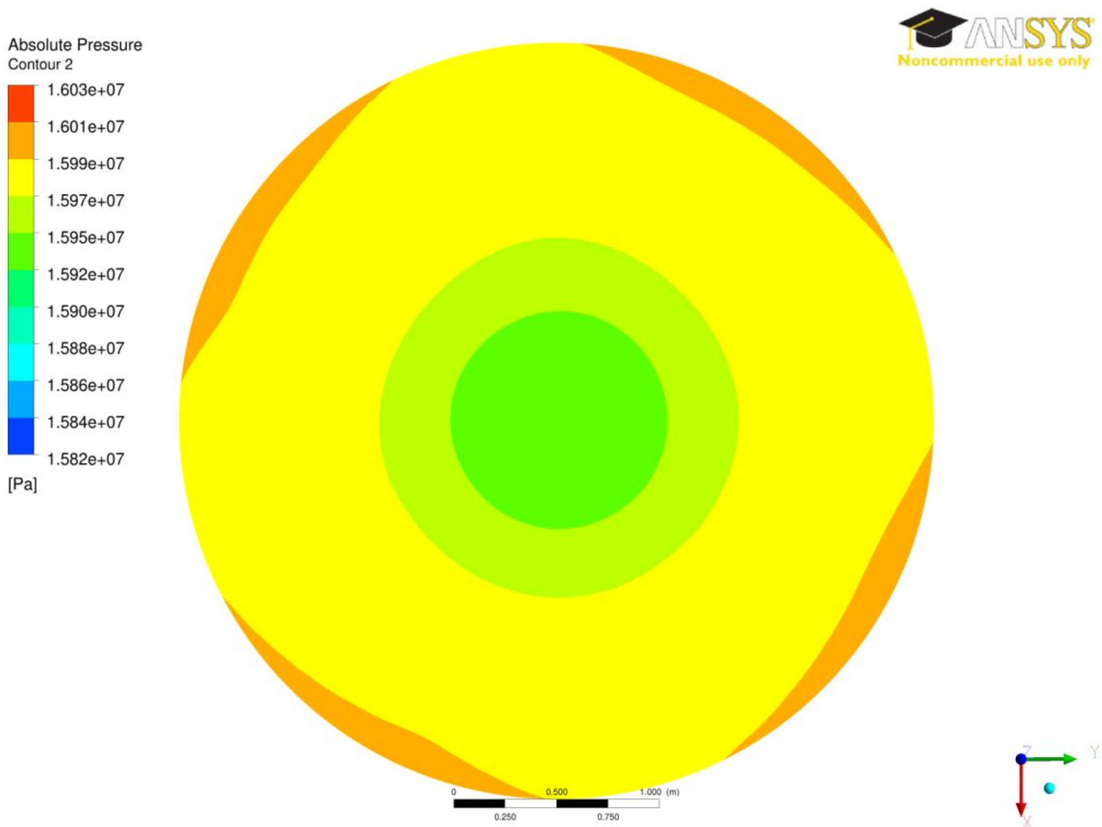

Figure 31: Absolute pressure in the core barrel bottom in the XY-plane at the approximate height of the guide tube openings

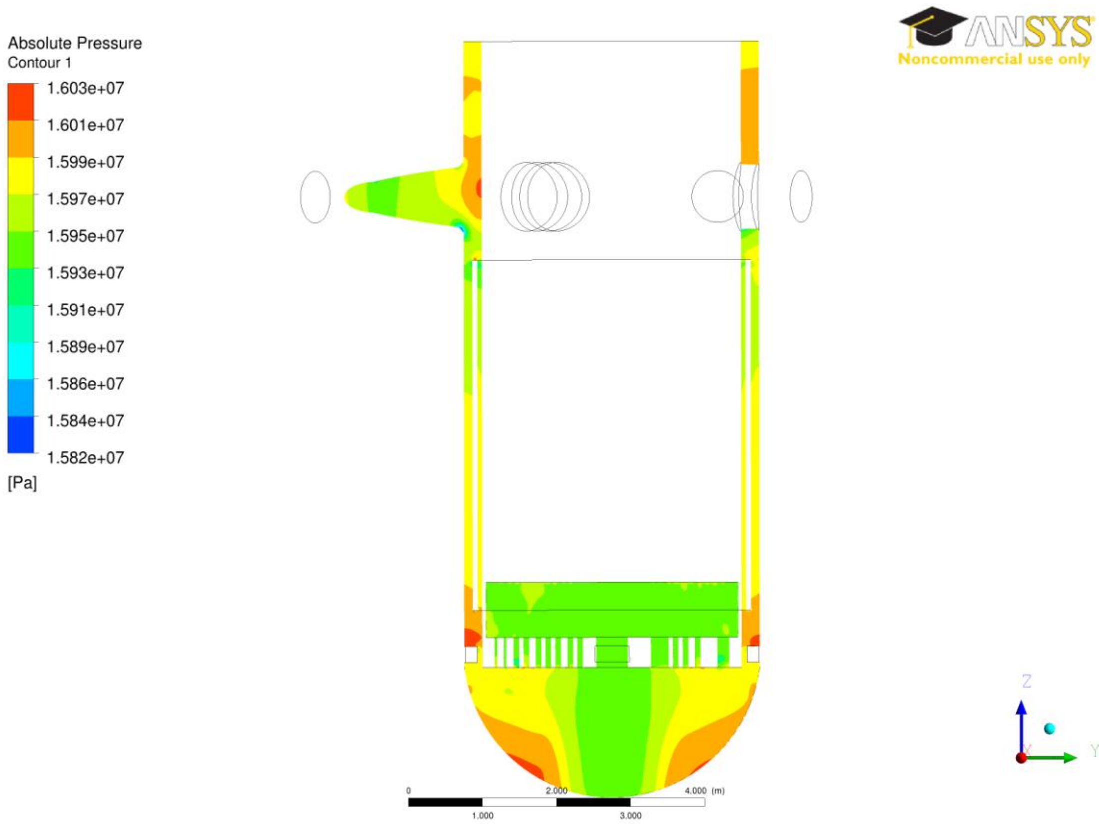

Figure 32: Absolute Pressure in the YZ-plane

Transient simulation of the full model

For this transient the same pendulum motion as described earlier with the 7.2 Hz frequency is used. The maximum displacement used is 1 mm simulating the maximum allowed gap on the lower radial supports and thus the maximum possible amplitude for the core barrel to move around.

The pressure versus time is shown in figure 33. From this figure it can be seen that the pressure in the different guide tubes are more closely grouped together with the exception of tube G9. This may be explained by looking at figure 31 and comparing with figure 34, there is a region with lower pressure in the vortex that is forming in the center of the RPV. Small fluctuations can be observed in all guide-tubes. The fluctuations are slightly larger than for the 1mm, simplified model case, this may be due to a slightly larger variation in pressure that is observed (compare figure 25 and 33).

In figure 34 the peak to peak amplitude is normalized with the amplitude at position B7. From this figure it is clear that the full model experiences more complex pressure variations than the simplified model. The Amplitude is still largest closest to the motion apex. The largest available amplitude in an available guide tube can be found in tube B7 and N8 with a pressure variation of about 0.002 MPa. The largest fluctuations still appears in the same positions as for the simplified model but with slightly larger amplitude. The amplitudes, maximum and minimum pressures for the different guide tubes locations can be found in table 6. The pressures are area averaged over a circular area with radius $r = 0.05$ m which should represent the opening area where the guide tube opens up inside the RPV.

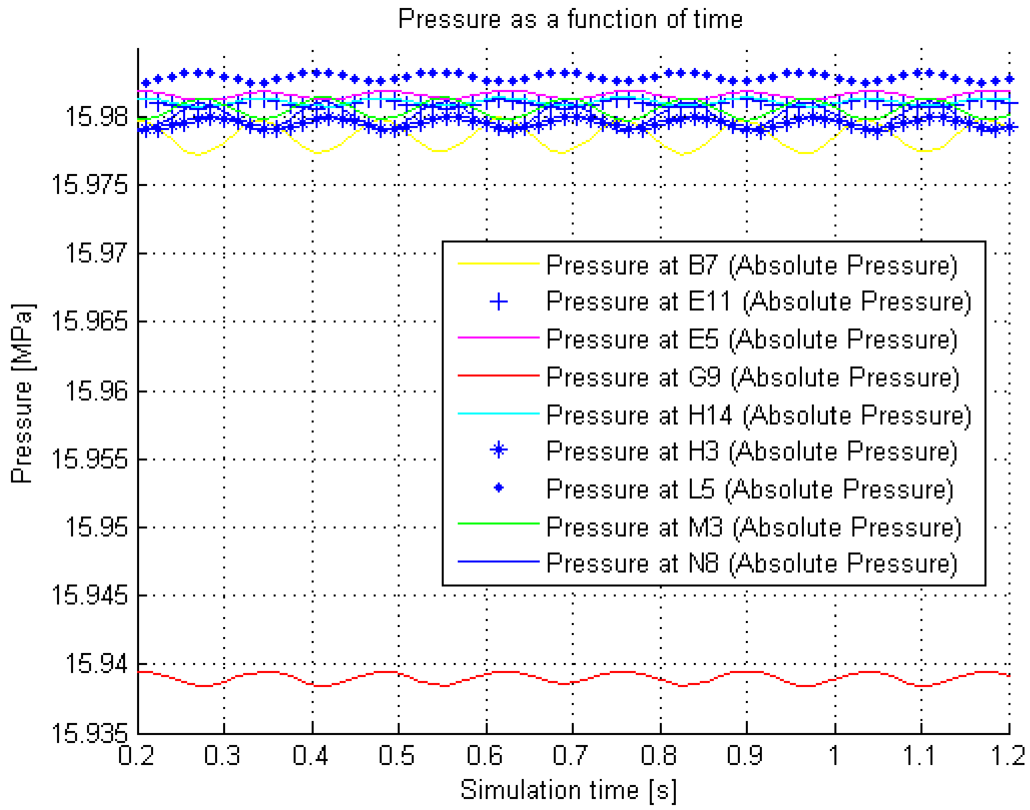

Figure 33: Pressure versus time for the full model with 1mm displacement and mass flow inlet

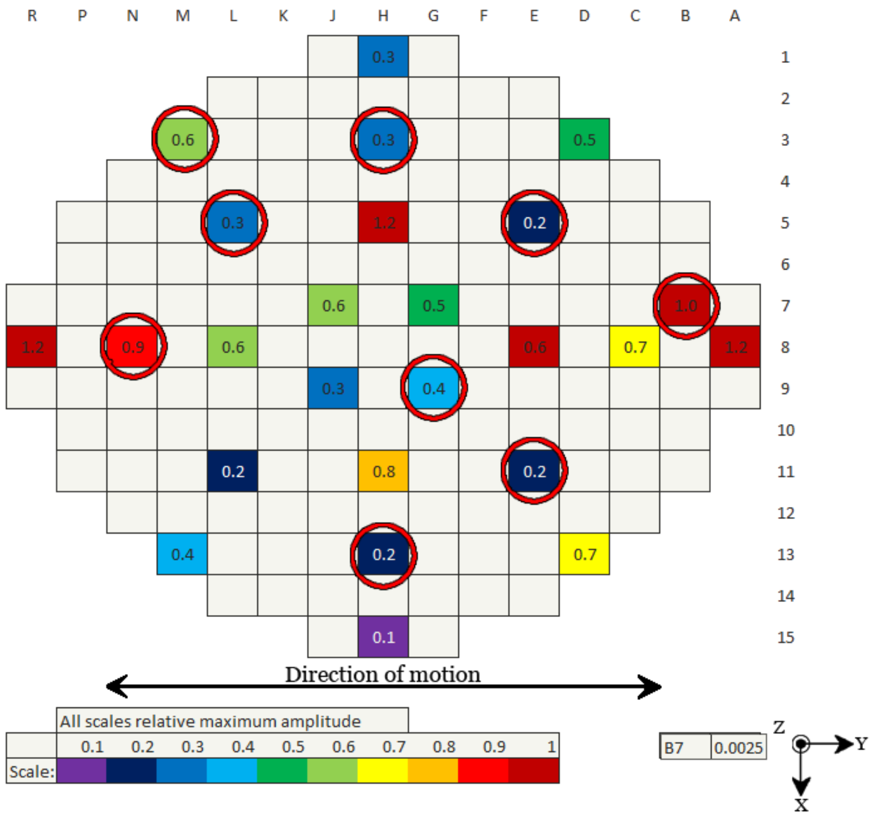

Figure 34: Relative pressure amplitude at the different guide tubes, relative guide tube B7. Full model, 1mm displacement and mass flow inlet, tubes available for measurements are circled in red

Table 6: Area averaged Amplitude, maximum and minimum pressures for different guide tube positions from the full model simulation

		Guide tube:								
	Pressures:	B7	E5	E11	G9	H3	H13	L5	M3	N8
Area averaged $\Delta t = 0.0025\ s$	Max [Mpa]:	15,9798	15,9819	15,9812	15,9395	15,9799	15,9813	15,9833	15,9813	15,9811
	Min [Mpa]:	15,9773	15,9813	15,9806	15,9385	15,9791	15,9808	15,9826	15,9798	15,9789
	Amplitude [Mpa]:	0,0024	0,0006	0,0006	0,0010	0,0008	0,0005	0,0007	0,0015	0,0022

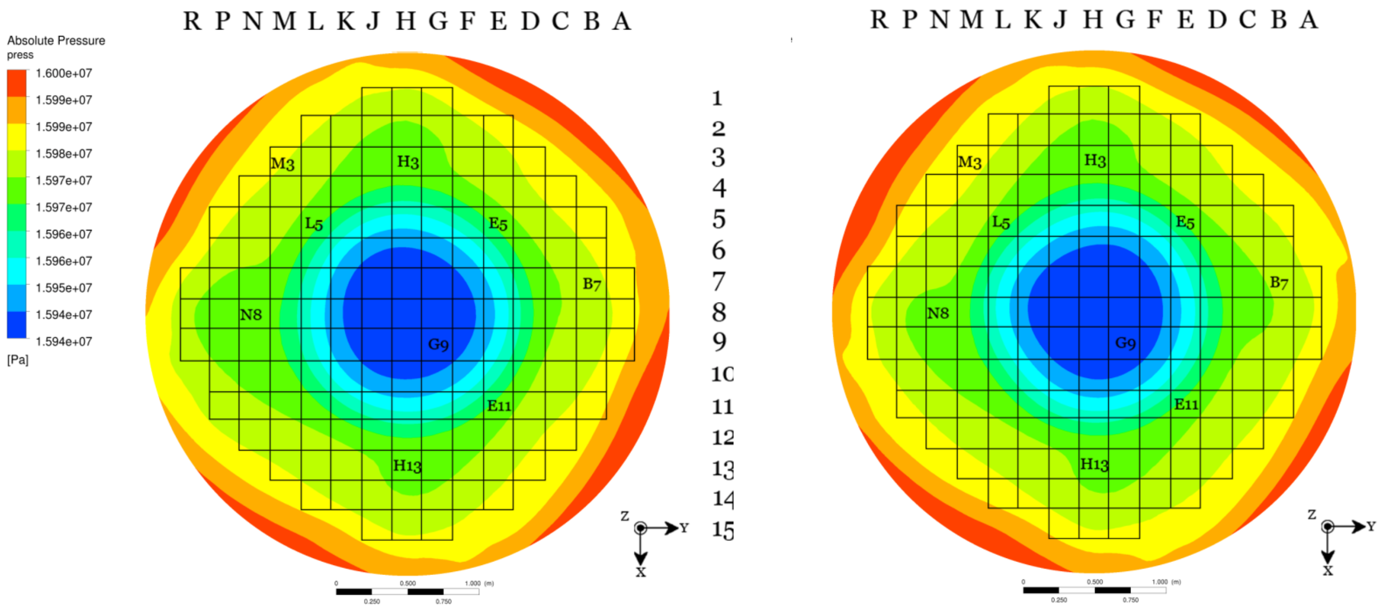

Figure 35: Absolute pressure for guide tube plane in the full model at two different time steps

Comparing the pressure distribution from two different time steps shows that the motion distorts the low pressure region in the vortex appearing in the RPV-center (see figure 35). This might explain the high amplitudes in some positions close to the center.

5. Conclusion

In this chapter the main conclusions from the results part together with recommendations for measurement positions will be presented. Further recommendation for future work will be given.

Location 2. in figure 3 was determined unsuitable for measuring pressure pulses emanating from core barrel movements due to the its location. Several other systems would probably influence the measurements to a high extent. This location is located near the PRZ which consists of a large vessel with a free water surface in contact with steam. It is believed that this steam pocket in the PRZ would dampen the pressure pulses to a high extent. It is therefore assumed that the reduction in domain size from excluding this position motivates its exclusion. By neglecting this point the computational domain can be cut before the core, effectively reducing the computational domain in half. Further by excluding the core, heat transfer may be neglected since the heat up of the coolant can be considered negligible before it enters the core.

From the simplified model of the reactor, a transient simulation was done with about 1.3M cells; the boundary layer is not resolved in this model. The model was constructed to see if a motion of the kind assumed in this work would generate pressure fluctuations at the points of interest in the geometry in question. From this model it is clear that even with a coarse mesh, fluctuations of the pressure occur at the locations of the guide tube openings.

Simulations with different boundary conditions show little effect of the inlet boundary condition, further the amplitude of the pressure pulses occurring seems to be almost linear for different core barrel displacements. The largest pressure pulses occur close to the periphery at maximum displacement of the core barrel, with lower amplitude closer to the center. Rotating the motion direction 90° moves the maximum amplitudes accordingly. This would suggest that the type and frequency of the motion/vibration is more important than the flow behavior for this model.

The size of the domain to be simulated made it hard to keep the amount of computational cells low; therefore the boundary layers where not resolved. This may give lower accuracy in the results of the flow. Thus the actual pressure may not be exact but the results should still predict where the pressure pulses should be the greatest. The mesh study showed a smaller change in the wall shear stress prediction between models as would be expected. The pressures at the points of interest showed very little change between meshes, less than 0.1 % which would indicate that the model still would work well for the purposes of this work.

Further the simulation from the full model shows a more complex behavior, where some pressure pulses are slightly offset. There are also larger pressure pulses occurring in the more central guide tube suggesting that the flow plays a larger role for the pulses in this more accurate model. Still the largest pressure amplitudes can be found close to the periphery as in the simplified model case.

The amplitude is found to be largest at position B7 for all simulations with the x-direction motion. The pressure pulse in these locations shows an peak to peak amplitude of about 0.002 MPa in the full model which should be possible to measure.

The result from both models thus suggests that the best place to take pressure measurements would be close to the periphery. The actual direction of the motion is not known, thus a second sensor should be put in a way that maximizes the chance of detection given an arbitrary motion. Since the current sensors are located in position H3, a second sensor should be put it in position B7. This position is close to the periphery and almost perpendicular to point H3 and would pick up motions the first sensor is less likely to do. Positions M3 and N8 would also be suitable for measurements.

5.1. Future work

For any future work or refinement it would be possible to compare the behavior of different turbulence models, for example SST which uses a k- ε model to describe the turbulence in the bulk flow and a k- ω model to describe the boundary layers. This model however needs $y^+ < 1$ which is not plausible given the computational resources in this work. Another interesting turbulence model is LES which does not use any time approximation which may make it useful for higher frequency vibrations.

Further the effect of compressibility should be investigated since it might have an effect on the results.

Finally given more computational power a finer mesh would be beneficial, resolving the boundary layers and better predicting the flow. Further mesh-studies are needed, determining the accuracy of low resolution. Given the rapid growth of computer performance such analysis has large future potential.

References

[1] World Nuclear Association. Nuclear Power Reactors. url: http://www.world-nuclear.org/info/inf32.html (visited on 06/06/2012)

[2] Nordlund. A. Introduction to Nuclear Reactors. Göteborg, Sweden: Chalmers Tekniska Högskola; 2010

[3] Vattenfall AB. OM VATTENFALL: Ringhals Historia i Sverige url: http://www.vattenfall.se/sv/ringhals-historia.htm?WT.ac=search_success (visited on 01/30/2012)

[4] Vattenfall AB. OM VATTENFALL: Kärnkraft - då nu och sedan. url: http://www.vattenfall.se/sv/ringhals-historia.htm?WT.ac=search_success (visited on 01/30/2012)

[5] Vattenfall AB. OM VATTENFALL: Ringhals Historia url: http://www.vattenfall.se/sv/ringhals-historia.htm?WT.ac=search_success (visited on 01/30/2012)

[6] Ringhals AB. Teknisk information om Ringhals.Väröbacka: Ringhals AB; 2011

[7] Versteeg. H.K. Malalasekera. W. An Introduction to Computational Fluid Dynamics - The Finite Volume Method, Second Edition. Harlow. England: Pearson Education Limited ; 2007

[8] Böttcher. M. Detailed CFX-5 Study Of The Coolant Mixing Within The Reactor Pressure Vessel Of A VVER-1000 Reactor During A Non-Symmetrical Heat-Up Test. Eggensteing-Leopoldshafen: Forchungszentrum Karlsruhe; -

[9] Dury. T.V. Hemström. B. Shepel. S.V. CFD simulation of the Vattenfall 1/5th-scale PWR model for boron dilution studies. Nuclear Engineering and Design 238. Elvsevier, Nuclear Engineering and Design 238.; 2008

[10] Höhne. T. Kliem. S. Modeling of a Buoancy-driven Flow Experiment in Pressurized Water Reactors Using CFD-Methods. Nuclear Engineering and Technology Vol. 39 No.4; 2007

[11] Bellet. S. Benhamadouche. S. Ferret. A. Secondary Flows In PWR Hot Legs, CFD Might Bring Some Light On The Flow Behavior. Toronto. Canada: The 14th International Topical Meeting on Nuclear Reactor Thermalhydraulics. NURETH-14:2011

[12]Morii. T. Hydraulic flow tests of APWR reactor internals for safety analysis. Tokyo: Elsevier; 2007

[13] Anwer. S.F. Hasan. N. Sanghi. S. Mukherjee. S. Computation of unsteady flows with moving boundaries using body fitted curvilinear moving grids. India: Elsevier Ltd; 2008

[14] White. F.M. Fluid Mechanics Sixth Edition. New York: McGraw-Hill; 2008

[15] Jiyuan. T. Guan. H.Y. Chaoqun. L. Computational Fluid Dynamics - A Practical Approach. USA: Elsevier; 2008

[16] Davidsson. L. An Introduction to Turbulence Models. Göteborg, Sweden: Chalmers University of Technology; 2003

[17] Flow Science Inc. Assessing Mesh Resolution for Boundary Layer Accuracy url: http://www.flow3d.com/resources/news_10/assessing-mesh-resolution-for-boundary-layer-accuracy.html (visited on 04/01/2012)

[18] ANSYS Inc. ANSYS CFX-Solver Theory Guide - Release 13.0. USA: ANSYS Inc.; 2011

[19] Onsala Ingenjörsbyrå. Tryckfördelning i RC för R2-4. Företagsintern rapport Ringhals AB; 2006

[20] National Institute of Standards Technology. Thermophysical Properties of Fluid Systems. url: http://webbook.nist.gov/chemistry/fluid/ (visited on 04/18/2012)

Appendix A: Ansys CFX intput file

The input file for transient simulations:

```
Setting up CFX Solver run ...


 +--------------------------------------------------------------------+
 |                                                                    |
 |                    CFX Command Language for Run                    |
 |                                                                    |
 +--------------------------------------------------------------------+

 LIBRARY:
   CEL:
     EXPRESSIONS:
       HZ = 7.2 [s^-1]
       Hbarrel = 8.438 [m]
       alfa = (pi/2)-acos(thetamax)
       arclength = radius*thetadisp*sinmotion
       radius = (z^2+y^2)^0.5
       rmax = (Hbarrel^2+ybarrel^2)^0.5
       sinmotion = sin(2*pi*t*HZ)
       thetadisp = asin(xdisp/(cos(alfa)*rmax))
       thetamax = asin(ybarrel/rmax)
       xdisp = 0.001 [m]
       ybarrel = 1.751 [m]
     END
   END
   MATERIAL: Varmt vatten
     Material Group = User
     Option = Pure Substance
     Thermodynamic State = Liquid
     PROPERTIES:
       Option = General Material
       EQUATION OF STATE:
         Density = 752.4 [kg m^-3]
         Molar Mass = 18.0153 [g mol^-1]
         Option = Value
       END
       SPECIFIC HEAT CAPACITY:
         Option = Value
         Specific Heat Capacity = 5180 [J kg^-1 K^-1]
         Specific Heat Type = Constant Pressure
       END
       DYNAMIC VISCOSITY:
         Dynamic Viscosity = 93.7e-6 [Pa s]
         Option = Value
       END
       THERMAL CONDUCTIVITY:
         Option = Value
         Thermal Conductivity = 0.586 [W m^-1 K^-1]
       END
       THERMAL EXPANSIVITY:
         Option = Value
         Thermal Expansivity = 0.00243 [K^-1]
       END
     END
   END
 END
 FLOW: Flow Analysis 1
   SOLUTION UNITS:
     Angle Units = [rad]
     Length Units = [m]
     Mass Units = [kg]
     Solid Angle Units = [sr]
     Temperature Units = [K]
     Time Units = [s]
   END
   ANALYSIS TYPE:
     Option = Transient
     EXTERNAL SOLVER COUPLING:
       Option = None
     END
     INITIAL TIME:
       Option = Automatic with Value
```

```
    Time = 0 [s]
  END
  TIME DURATION:
    Option = Total Time
    Total Time = 8 [s]
  END
  TIME STEPS:
    Option = Timesteps
    Timesteps = 0.005 [s]
  END
END
DOMAIN: Default Domain
  Coord Frame = Coord 0
  Domain Type = Fluid
  Location = Primitive 3D, Primitive 3D A, Primitive 3D B, Primitive 3D C
  BOUNDARY: Deformedwall
    Boundary Type = WALL
    Location = inspecifiedmotionparts
    BOUNDARY CONDITIONS:
      MASS AND MOMENTUM:
        Option = No Slip Wall
      END
      MESH MOTION:
        Option = Unspecified
      END
      WALL ROUGHNESS:
        Option = Smooth Wall
      END
    END
  END
  BOUNDARY: Inlet 1
    Boundary Type = INLET
    Location = IN1
    BOUNDARY CONDITIONS:
      FLOW DIRECTION:
        Option = Normal to Boundary Condition
      END
      FLOW REGIME:
        Option = Subsonic
      END
      MASS AND MOMENTUM:
        Mass Flow Rate = 4582.333 [kg s^-1]
        Option = Mass Flow Rate
      END
      MESH MOTION:
        Option = Stationary
      END
      TURBULENCE:
        Option = Medium Intensity and Eddy Viscosity Ratio
      END
    END
  END
  BOUNDARY: Inlet 2
    Boundary Type = INLET
    Location = IN2
    BOUNDARY CONDITIONS:
      FLOW DIRECTION:
        Option = Normal to Boundary Condition
      END
      FLOW REGIME:
        Option = Subsonic
      END
      MASS AND MOMENTUM:
        Mass Flow Rate = 4582.333 [kg s^-1]
        Option = Mass Flow Rate
      END
      MESH MOTION:
        Option = Stationary
      END
      TURBULENCE:
        Option = Medium Intensity and Eddy Viscosity Ratio
      END
    END
  END
  BOUNDARY: Inlet 3
    Boundary Type = INLET
    Location = IN3
```

```
  BOUNDARY CONDITIONS:
    FLOW DIRECTION:
      Option = Normal to Boundary Condition
    END
    FLOW REGIME:
      Option = Subsonic
    END
    MASS AND MOMENTUM:
      Mass Flow Rate = 4582.333 [kg s^-1]
      Option = Mass Flow Rate
    END
    MESH MOTION:
      Option = Stationary
    END
    TURBULENCE:
      Option = Medium Intensity and Eddy Viscosity Ratio
    END
  END
END
BOUNDARY: Moving Walls
  Boundary Type = WALL
  Location = \
    Core_barrel_center_holes,Core_barrel_large_holse,Core_barrel_small_ho\
    les,Guide_Tubes,Holes_close_to_center,Shield,Inner_wall_lower,Inner_w\
    all_lower \
    1,Inner_wall_upper,Lower_core_barrel_plate,Upper_core_barrel_plate,Ou\
    tlet_wall
  BOUNDARY CONDITIONS:
    MASS AND MOMENTUM:
      Option = No Slip Wall
    END
    MESH MOTION:
      Option = Specified Displacement
      DISPLACEMENT:
        Displacement Axial Component = 0 [m]
        Displacement Theta Component = arclength
        Displacement r Component = 0 [m]
        Option = Cylindrical Components
        AXIS DEFINITION:
          Option = Coordinate Axis
          Rotation Axis = Coord 0.1
        END
      END
    END
    WALL ROUGHNESS:
      Option = Smooth Wall
    END
  END
END
BOUNDARY: Outer Walls
  Boundary Type = WALL
  Location = \
    Inlet_pipes,Half_sphere,Outer_wall_lower_and_sphere,Outer_wall_middle\
    ,Outer_wall_upper
  BOUNDARY CONDITIONS:
    MASS AND MOMENTUM:
      Option = No Slip Wall
    END
    MESH MOTION:
      Option = Stationary
    END
    WALL ROUGHNESS:
      Option = Smooth Wall
    END
  END
END
BOUNDARY: Outlet
  Boundary Type = OUTLET
  Location = Outlet
  BOUNDARY CONDITIONS:
    FLOW REGIME:
      Option = Subsonic
    END
    MASS AND MOMENTUM:
      Option = Average Static Pressure
      Pressure Profile Blend = 0.05
      Relative Pressure = 8.7 [bar]
```

```
    END
    MESH MOTION:
      Option = Unspecified
    END
    PRESSURE AVERAGING:
      Option = Average Over Whole Outlet
    END
  END
END
DOMAIN MODELS:
  BUOYANCY MODEL:
    Buoyancy Reference Temperature = 287 [C]
    Gravity X Component = 0 [m s^-2]
    Gravity Y Component = 0 [m s^-2]
    Gravity Z Component = -9.82 [m s^-2]
    Option = Buoyant
    BUOYANCY REFERENCE LOCATION:
      Cartesian Coordinates = 0 [m], 0 [m], -2.093 [m]
      Option = Cartesian Coordinates
    END
  END
  DOMAIN MOTION:
    Option = Stationary
  END
  MESH DEFORMATION:
    Option = Regions of Motion Specified
    MESH MOTION MODEL:
      Option = Displacement Diffusion
      MESH STIFFNESS:
        Option = Increase near Small Volumes
        Stiffness Model Exponent = 10
      END
    END
  END
  REFERENCE PRESSURE:
    Reference Pressure = 150 [bar]
  END
END
FLUID DEFINITION: Fluid 1
  Material = Varmt vatten
  Option = Material Library
  MORPHOLOGY:
    Option = Continuous Fluid
  END
END
FLUID MODELS:
  COMBUSTION MODEL:
    Option = None
  END
  HEAT TRANSFER MODEL:
    Fluid Temperature = 287 [C]
    Option = Isothermal
  END
  THERMAL RADIATION MODEL:
    Option = None
  END
  TURBULENCE MODEL:
    Option = k epsilon
    BUOYANCY TURBULENCE:
      Option = None
    END
  END
  TURBULENT WALL FUNCTIONS:
    Option = Scalable
  END
END
INITIALISATION:
  Option = Automatic
  INITIAL CONDITIONS:
    Velocity Type = Cartesian
    CARTESIAN VELOCITY COMPONENTS:
      Option = Automatic with Value
      U = 0 [m s^-1]
      V = 0 [m s^-1]
      W = -5 [m s^-1]
    END
    STATIC PRESSURE:
```

```
        Option = Automatic with Value
        Relative Pressure = 9 [bar]
      END
      TURBULENCE INITIAL CONDITIONS:
        Option = Medium Intensity and Eddy Viscosity Ratio
      END
    END
  END
END
OUTPUT CONTROL:
  BACKUP RESULTS: Backup Results 1
    File Compression Level = Default
    Option = Standard
    OUTPUT FREQUENCY:
      Option = Timestep Interval
      Timestep Interval = 1
    END
  END
  MONITOR OBJECTS:
    MONITOR BALANCES:
      Option = Full
    END
    MONITOR FORCES:
      Option = Full
    END
    MONITOR PARTICLES:
      Option = Full
    END
    MONITOR POINT: Pressure at A8
      Cartesian Coordinates = 0 [m], 1.505 [m], -8.85 [m]
      Option = Cartesian Coordinates
      Output Variables List = Absolute Pressure
    END
    MONITOR POINT: Pressure at B7
      Cartesian Coordinates = -0.215 [m], 1.29 [m], -9.0444 [m]
      Option = Cartesian Coordinates
      Output Variables List = Absolute Pressure
    END
    MONITOR POINT: Pressure at C8
      Cartesian Coordinates = 0 [m], 1.075 [m], -9.217 [m]
      Option = Cartesian Coordinates
      Output Variables List = Absolute Pressure
    END
    MONITOR POINT: Pressure at D13
      Cartesian Coordinates = 1.075 [m], 0.86 [m], -8.982 [m]
      Option = Cartesian Coordinates
      Output Variables List = Absolute Pressure
    END
    MONITOR POINT: Pressure at D3
      Cartesian Coordinates = -1.075 [m], 0.86 [m], -8.982 [m]
      Option = Cartesian Coordinates
      Output Variables List = Absolute Pressure
    END
    MONITOR POINT: Pressure at E11
      Cartesian Coordinates = 0.645 [m], 0.645 [m], -9.3094 [m]
      Option = Cartesian Coordinates
      Output Variables List = Absolute Pressure
    END
    MONITOR POINT: Pressure at E5
      Cartesian Coordinates = -0.645 [m], 0.645 [m], -9.3094 [m]
      Option = Cartesian Coordinates
      Output Variables List = Absolute Pressure
    END
    MONITOR POINT: Pressure at E8
      Cartesian Coordinates = 0 [m], 0.645 [m], -9.422 [m]
      Option = Cartesian Coordinates
      Output Variables List = Absolute Pressure
    END
    MONITOR POINT: Pressure at G7
      Cartesian Coordinates = -0.215 [m], 0.215 [m], -9.505 [m]
      Option = Cartesian Coordinates
      Output Variables List = Absolute Pressure
    END
    MONITOR POINT: Pressure at G9
      Cartesian Coordinates = 0.21504 [m], 0.21504 [m], -9.5054 [m]
      Option = Cartesian Coordinates
      Output Variables List = Absolute Pressure
```

```
END
MONITOR POINT: Pressure at H1
  Cartesian Coordinates = -1.505 [m], 0 [m], -8.85 [m]
  Option = Cartesian Coordinates
  Output Variables List = Absolute Pressure
END
MONITOR POINT: Pressure at H11
  Cartesian Coordinates = 0.645 [m], 0 [m], -9.422 [m]
  Option = Cartesian Coordinates
  Output Variables List = Absolute Pressure
END
MONITOR POINT: Pressure at H14
  Cartesian Coordinates = 1.075 [m], 0 [m], -9.2166 [m]
  Option = Cartesian Coordinates
  Output Variables List = Absolute Pressure
END
MONITOR POINT: Pressure at H15
  Cartesian Coordinates = 1.505 [m], 0 [m], -8.85 [m]
  Option = Cartesian Coordinates
  Output Variables List = Absolute Pressure
END
MONITOR POINT: Pressure at H3
  Cartesian Coordinates = -1.075 [m], 0 [m], -9.2166 [m]
  Option = Cartesian Coordinates
  Output Variables List = Absolute Pressure
END
MONITOR POINT: Pressure at H5
  Cartesian Coordinates = -0.645 [m], 0 [m], -9.422 [m]
  Option = Cartesian Coordinates
  Output Variables List = Absolute Pressure
END
MONITOR POINT: Pressure at Inlet
  Expression Value = (areaAve(Absolute Pressure \
    )@REGION:IN1+areaAve(Absolute Pressure \
    )@REGION:IN2+areaAve(Absolute Pressure )@REGION:IN3)/3
  Option = Expression
END
MONITOR POINT: Pressure at J7
  Cartesian Coordinates = -0.215 [m], -0.215 [m], -9.505 [m]
  Option = Cartesian Coordinates
  Output Variables List = Absolute Pressure
END
MONITOR POINT: Pressure at J9
  Cartesian Coordinates = 0.215 [m], -0.215 [m], -9.505 [m]
  Option = Cartesian Coordinates
  Output Variables List = Absolute Pressure
END
MONITOR POINT: Pressure at L11
  Cartesian Coordinates = 0.645 [m], -0.645 [m], -9.309 [m]
  Option = Cartesian Coordinates
  Output Variables List = Absolute Pressure
END
MONITOR POINT: Pressure at L5
  Cartesian Coordinates = -0.645 [m], -0.645 [m], -9.3094 [m]
  Option = Cartesian Coordinates
  Output Variables List = Absolute Pressure
END
MONITOR POINT: Pressure at L8
  Cartesian Coordinates = 0 [m], -0.645 [m], -9.422 [m]
  Option = Cartesian Coordinates
  Output Variables List = Absolute Pressure
END
MONITOR POINT: Pressure at M13
  Cartesian Coordinates = 1.075 [m], -0.86 [m], -8.982 [m]
  Option = Cartesian Coordinates
  Output Variables List = Absolute Pressure
END
MONITOR POINT: Pressure at M3
  Cartesian Coordinates = -1.07518 [m], -0.860156 [m], -8.9824 [m]
  Option = Cartesian Coordinates
  Output Variables List = Absolute Pressure
END
MONITOR POINT: Pressure at N8
  Cartesian Coordinates = 0 [m], -1.075 [m], -9.2166 [m]
  Option = Cartesian Coordinates
  Output Variables List = Absolute Pressure
END
```

```
      MONITOR POINT: Pressure at R8
        Cartesian Coordinates = 0 [m], -1.505 [m], -8.85 [m]
        Option = Cartesian Coordinates
        Output Variables List = Absolute Pressure
      END
      MONITOR POINT: Pressure att sphere center
        Cartesian Coordinates = 0 [m], 0 [m], -9.5 [m]
        Option = Cartesian Coordinates
        Output Variables List = Absolute Pressure
      END
      MONITOR RESIDUALS:
        Option = Full
      END
      MONITOR TOTALS:
        Option = Full
      END
    END
    RESULTS:
      File Compression Level = Default
      Option = Standard
    END
    TRANSIENT RESULTS: Transient Results 1
      File Compression Level = Default
      Option = Standard
      OUTPUT FREQUENCY:
        Option = Timestep Interval
        Timestep Interval = 6
      END
    END
  END
  SOLVER CONTROL:
    Turbulence Numerics = High Resolution
    ADVECTION SCHEME:
      Option = High Resolution
    END
    CONVERGENCE CONTROL:
      Maximum Number of Coefficient Loops = 20
      Minimum Number of Coefficient Loops = 5
      Timescale Control = Coefficient Loops
    END
    CONVERGENCE CRITERIA:
      Residual Target = 1e-06
      Residual Type = RMS
    END
    TRANSIENT SCHEME:
      Option = Second Order Backward Euler
      TIMESTEP INITIALISATION:
        Option = Automatic
      END
    END
  END
END
COMMAND FILE:
  Version = 14.0
  Results Version = 14.0
END
SIMULATION CONTROL:
  EXECUTION CONTROL:
    EXECUTABLE SELECTION:
      Double Precision = On
    END
    INTERPOLATOR STEP CONTROL:
      Runtime Priority = Standard
      MEMORY CONTROL:
        Memory Allocation Factor = 1.0
      END
    END
    PARALLEL HOST LIBRARY:
      HOST DEFINITION: eht11048
        Host Architecture String = linux-amd64
        Installation Root = /fs/soft/ansys/v%v/CFX
      END
    END
    PARTITIONER STEP CONTROL:
      Multidomain Option = Independent Partitioning
      Runtime Priority = Standard
      EXECUTABLE SELECTION:
```

```
      Use Large Problem Partitioner = Off
    END
    MEMORY CONTROL:
      Memory Allocation Factor = 1.0
    END
    PARTITIONING TYPE:
      MeTiS Type = k-way
      Option = MeTiS
      Partition Size Rule = Automatic
      Partition Weight Factors = 0.25000, 0.25000, 0.25000, 0.25000
    END
  END
  RUN DEFINITION:
    Run Mode = Full
    Solver Input File = \
      /fs/hem/ehtxcnm/full_model/No_layers_4M/1mm_trans_press_in/4M_1mm_tra\
      ns_press_in.def
    INITIAL VALUES SPECIFICATION:
      INITIAL VALUES CONTROL:
        Continue History From = Initial Values 1
        Use Mesh From = Solver Input File
      END
      INITIAL VALUES: Initial Values 1
        File Name = \
          /fs/hem/ehtxcnm/full_model/No_layers_4M/5M_mesh_9L_2nd_SS_001.res
        Option = Results File
      END
    END
  END
  SOLVER STEP CONTROL:
    Runtime Priority = Standard
    MEMORY CONTROL:
      Memory Allocation Factor = 1.0
    END
    PARALLEL ENVIRONMENT:
      Number of Processes = 4
      Start Method = MPICH Local Parallel
      Parallel Host List = eht11048*4
    END
  END
END
END
```

Appendix B: Full table data for transient simulations

Table B 1: Amplitudes for the different guide tube positions

Simplified model										Full model
Boundary condition:	Mass flow inlet						Pressure inlet			Mass flow inlet
Displacement [mm]:	0,5	1	2,5	5	10	15	1	5	10	1
Pressure amplitude at [Mpa]:										
Available:										
B7	0,0005	0,0009	0,0022	0,0045	0,0089	0,0135	0,0009	0,0042	0,0085	0,0024
E5	0,0002	0,0004	0,0009	0,0018	0,0036	0,0056	0,0004	0,0018	0,0036	0,0006
E11	0,0001	0,0003	0,0007	0,0015	0,0030	0,0045	0,0003	0,0015	0,0030	0,0006
G9	0,0000	0,0001	0,0002	0,0004	0,0008	0,0014	0,0001	0,0005	0,0010	0,0010
H3	0,0000	0,0000	0,0001	0,0002	0,0004	0,0008	0,0000	0,0002	0,0006	0,0008
H13	0,0000	0,0000	0,0001	0,0002	0,0005	0,0010	0,0001	0,0003	0,0007	0,0005
L5	0,0002	0,0004	0,0009	0,0018	0,0037	0,0056	0,0004	0,0017	0,0034	0,0007
M3	0,0003	0,0006	0,0014	0,0027	0,0054	0,0083	0,0005	0,0025	0,0051	0,0015
N8	0,0004	0,0007	0,0017	0,0034	0,0067	0,0100	0,0006	0,0031	0,0061	0,0022
Aditional positions:										
A8	0,0006	0,0012	0,0031	0,0062	0,0123	0,0188	-	-	-	0,0031
C8	0,0003	0,0007	0,0017	0,0034	0,0067	0,0102	-	-	-	0,0016
D13	0,0003	0,0007	0,0017	0,0033	0,0066	0,0099	-	-	-	0,0017
E8	0,0002	0,0003	0,0008	0,0016	0,0031	0,0047	-	-	-	0,0023
G7	0,0001	0,0001	0,0003	0,0006	0,0013	0,0020	-	-	-	0,0012
H1	0,0000	0,0000	0,0001	0,0001	0,0004	0,0007	-	-	-	0,0004
H11	0,0000	0,0000	0,0001	0,0002	0,0004	0,0007	-	-	-	0,0021
H15	0,0000	0,0000	0,0001	0,0001	0,0003	0,0006	-	-	-	0,0003
H5	0,0000	0,0000	0,0001	0,0001	0,0003	0,0006	-	-	-	0,0030
J7	0,0001	0,0001	0,0003	0,0006	0,0011	0,0016	-	-	-	0,0015
J9	0,0001	0,0001	0,0003	0,0006	0,0012	0,0018	-	-	-	0,0007
L11	0,0000	0,0000	0,0001	0,0002	0,0004	0,0007	-	-	-	0,0005
L8	0,0002	0,0004	0,0009	0,0018	0,0036	0,0054	-	-	-	0,0014
M13	0,0004	0,0007	0,0017	0,0035	0,0069	0,0103	-	-	-	0,0009
R8	0,0006	0,0012	0,0028	0,0057	0,0113	0,0170	-	-	-	0,0031

Appendix C: Simulation pressure figures

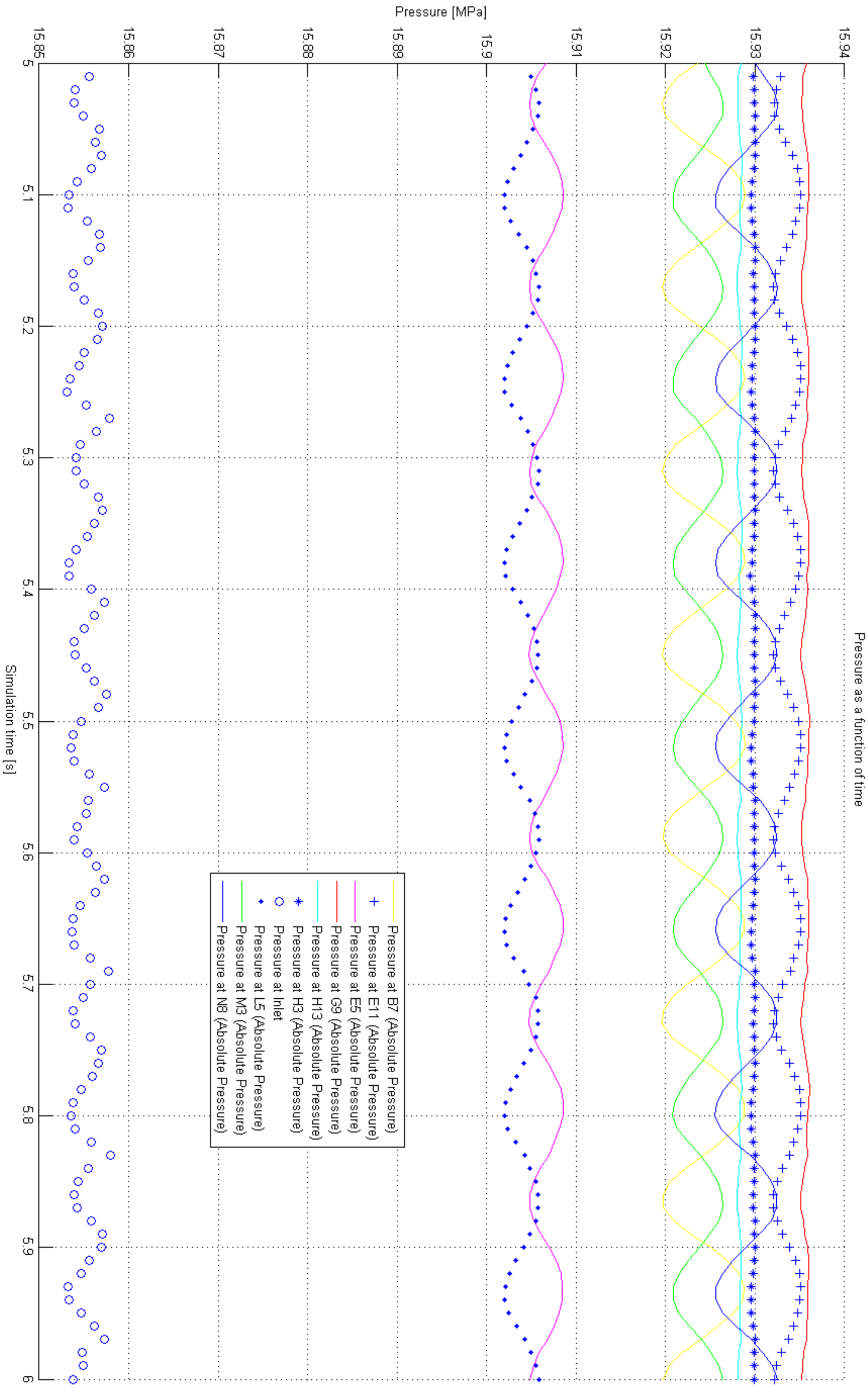

Figure C 1: Pressure versus amplitude for simplified model with 10 mm displacement and mass flow inlet

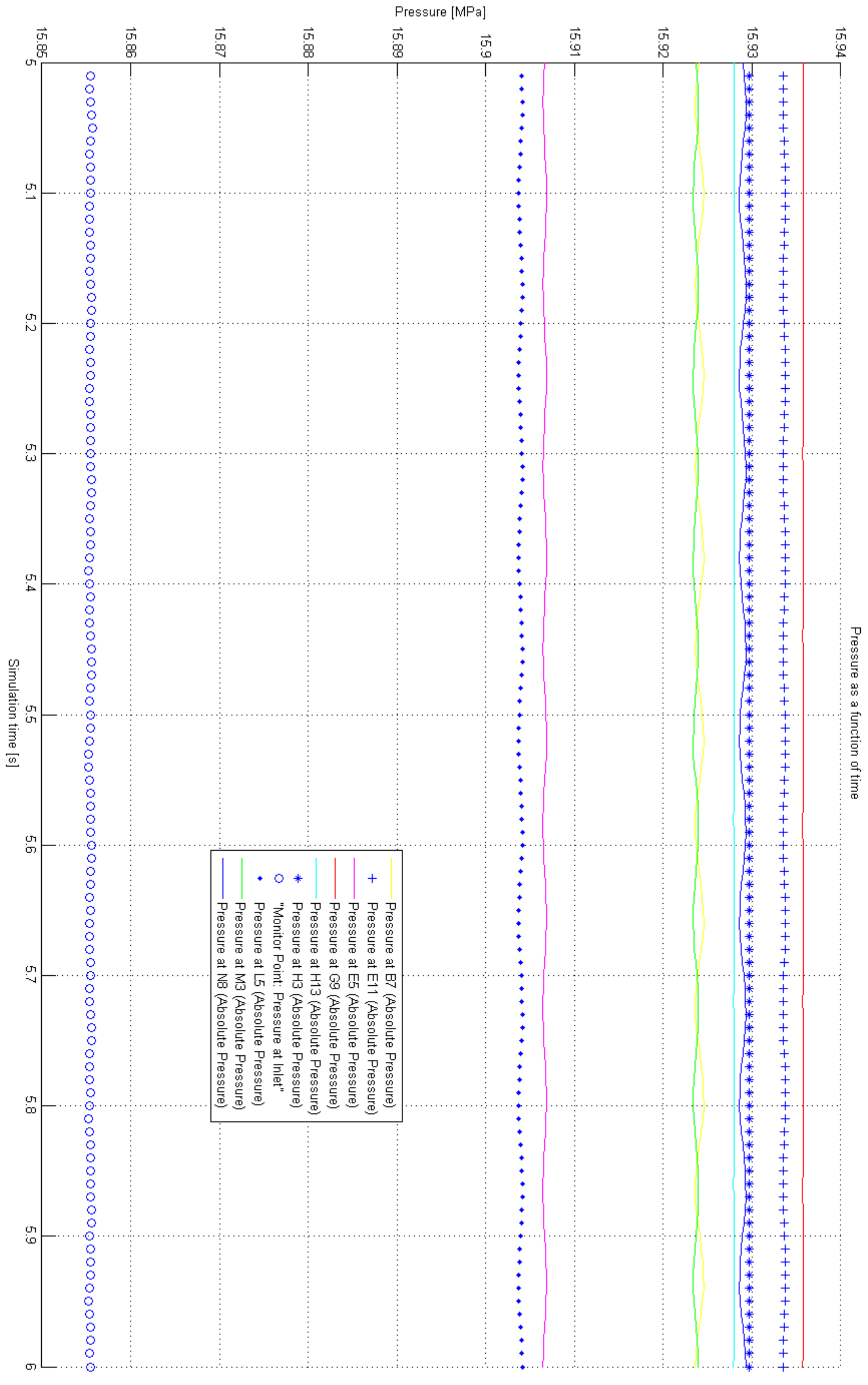

Figure C 2: Pressure versus amplitude for simplified model with 1 mm displacement and mass flow inlet

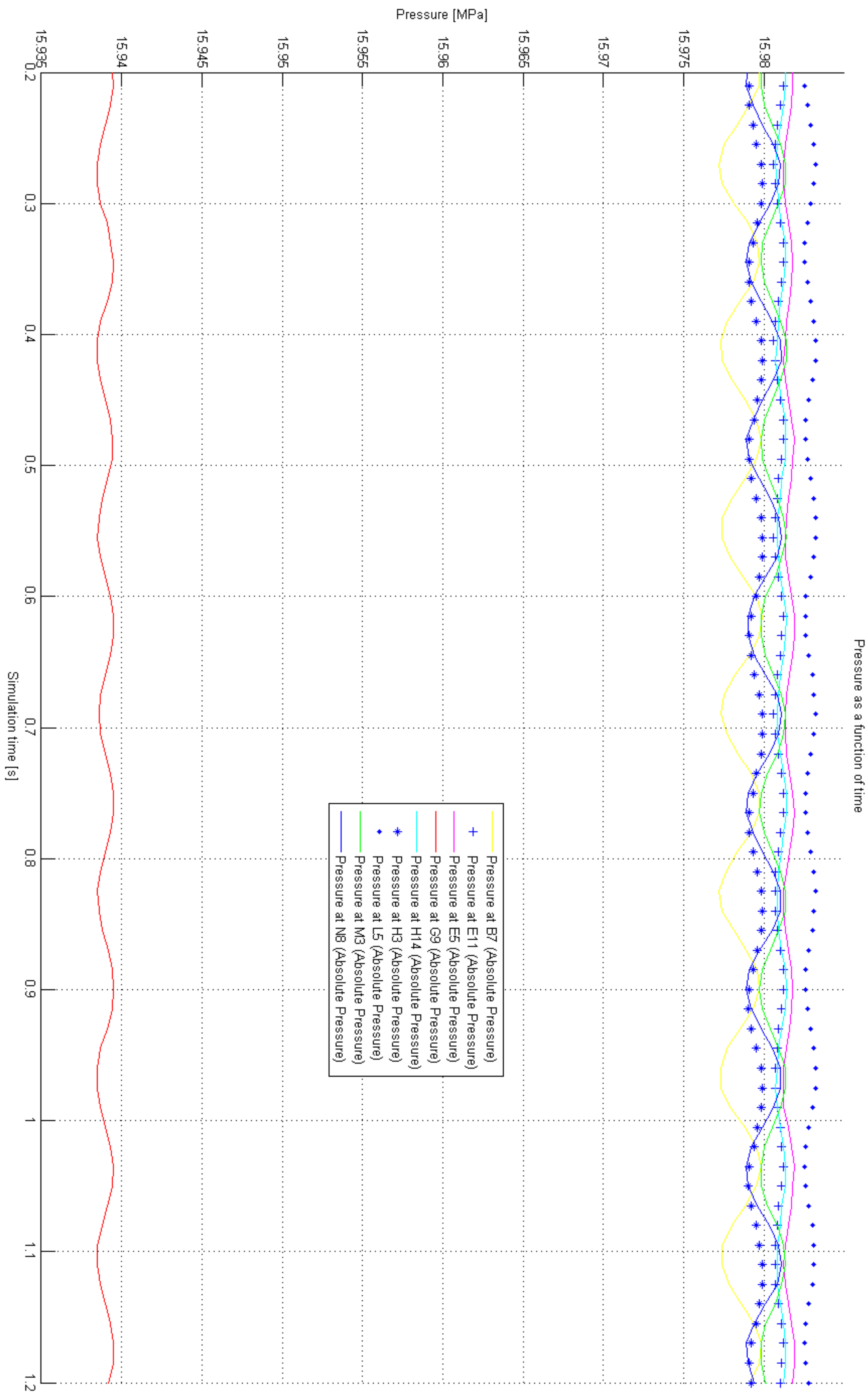

Figure C 3: Pressure versus amplitude for full model with 1mm displacement and mass flow inlet

Appendix D: Flow behavior of the full model

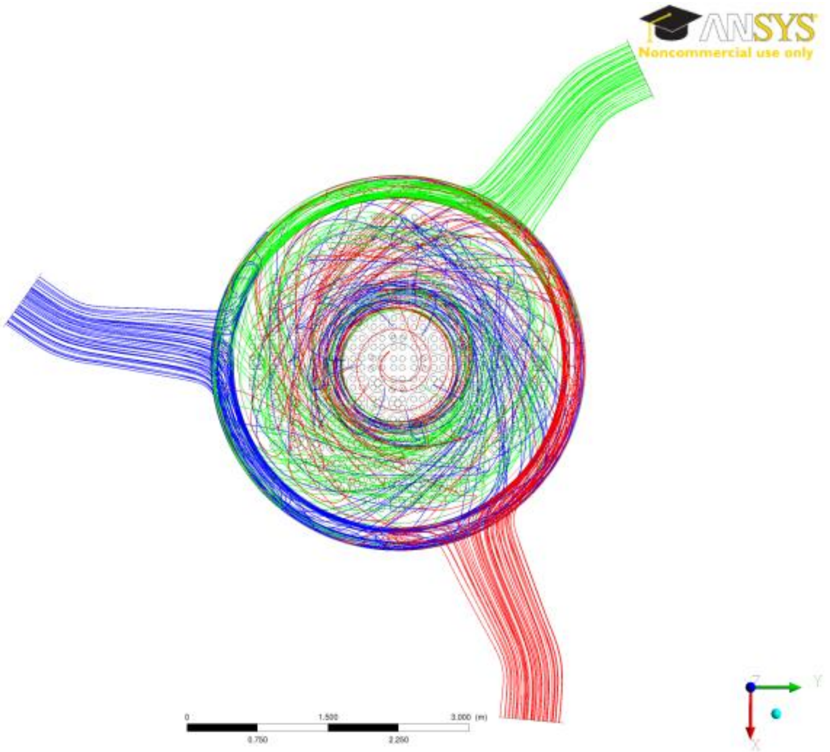

Figure D 1: Stream lines colored by inlet, (red, green and blue for inlets 1, 2 and 3 respectively) for the full model viewed from below

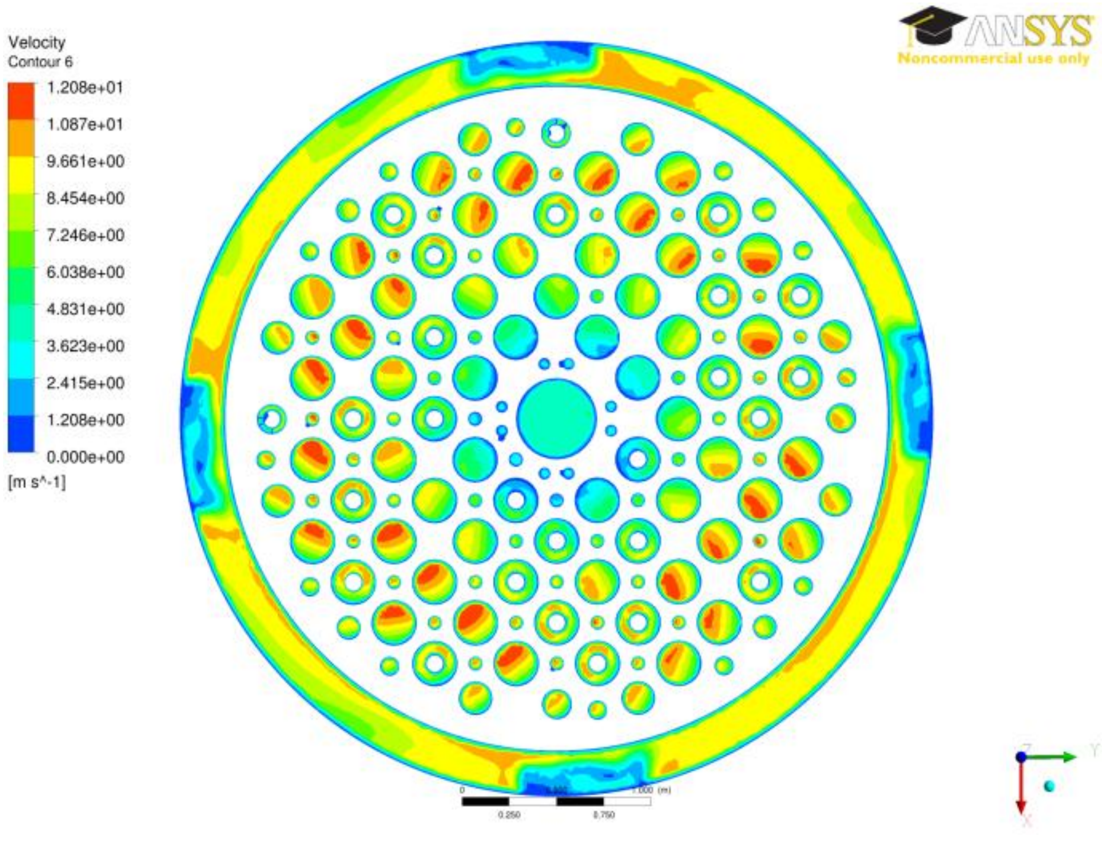

Figure D 2: Velocity at core barrel bottom in the XY-plane

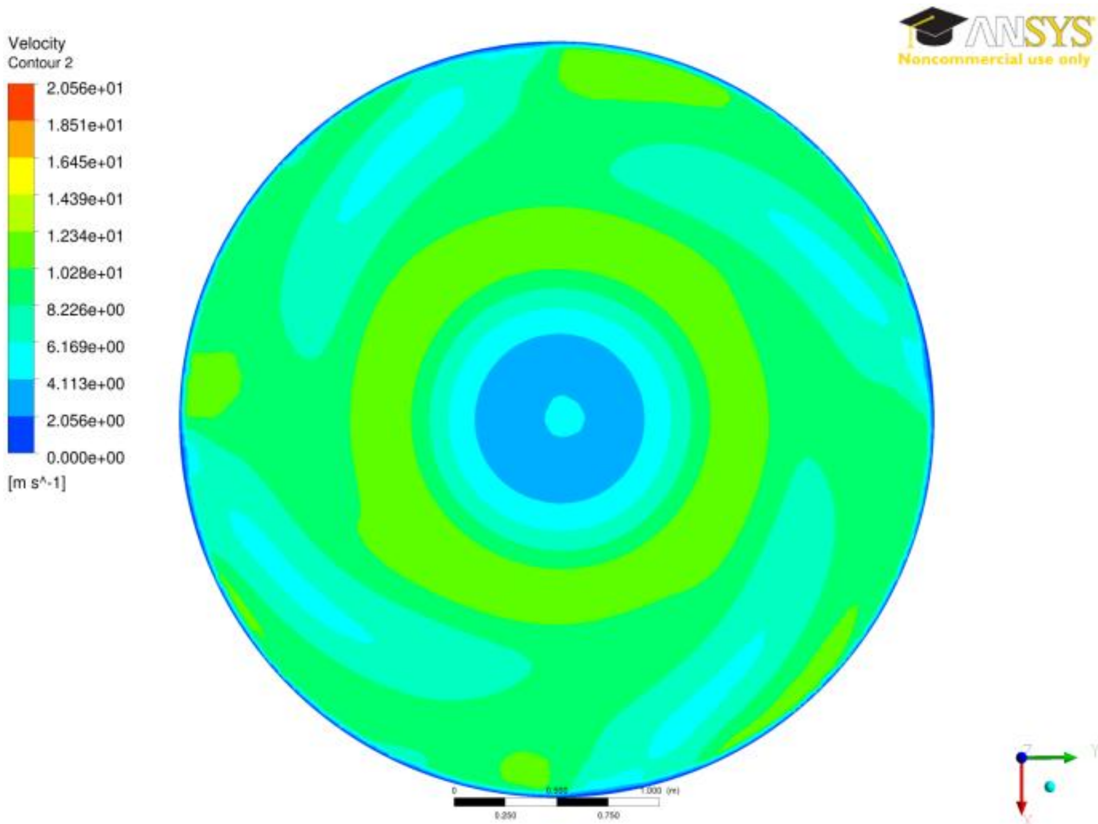

Figure D 3: Velocity in the core barrel bottom in the XY-plane at the approximate height of the guide tube outlets

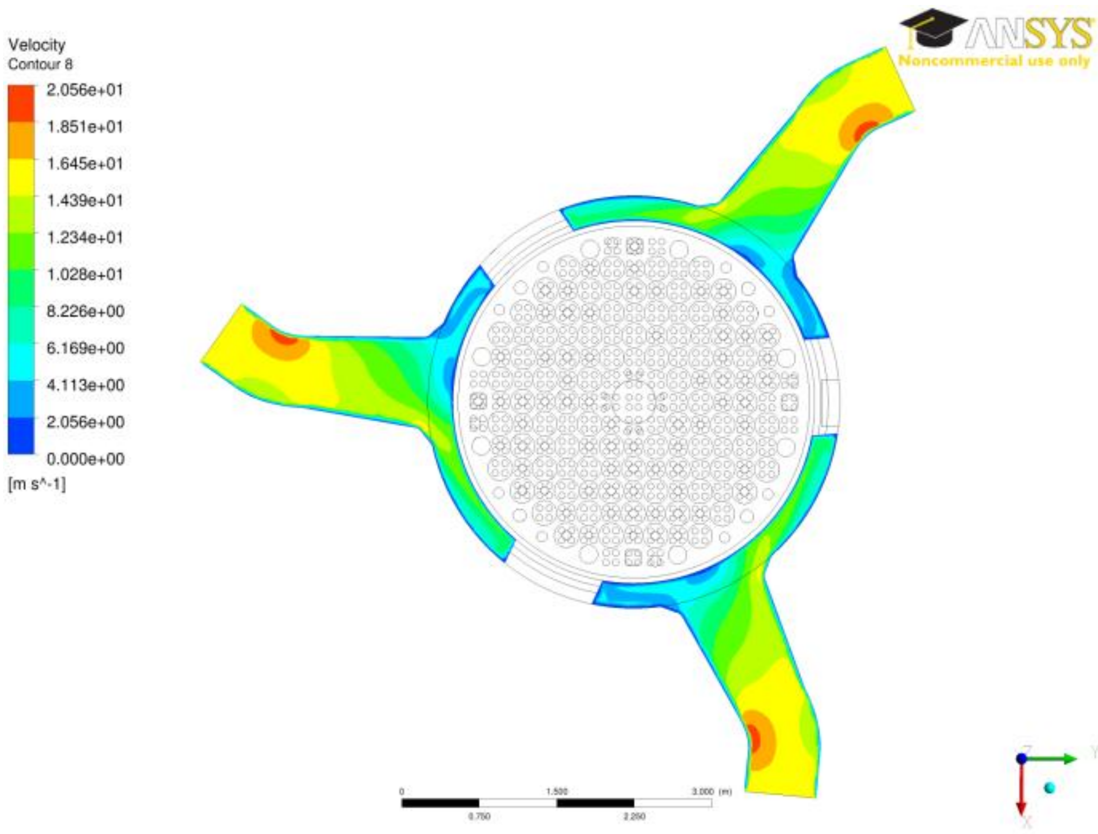

Figure D 4: Velocity in the XY-plane at the height of the inlets

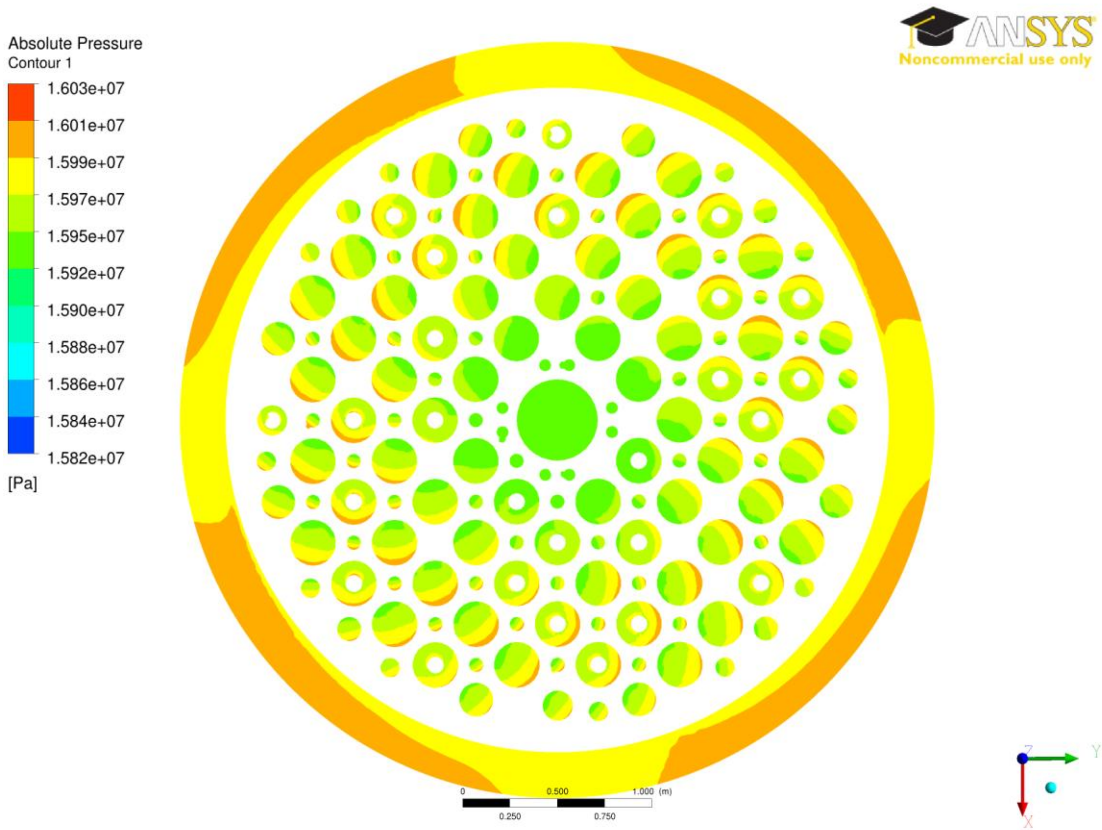

Figure D 5: Absolute pressure at core barrel bottom in the YX-plane

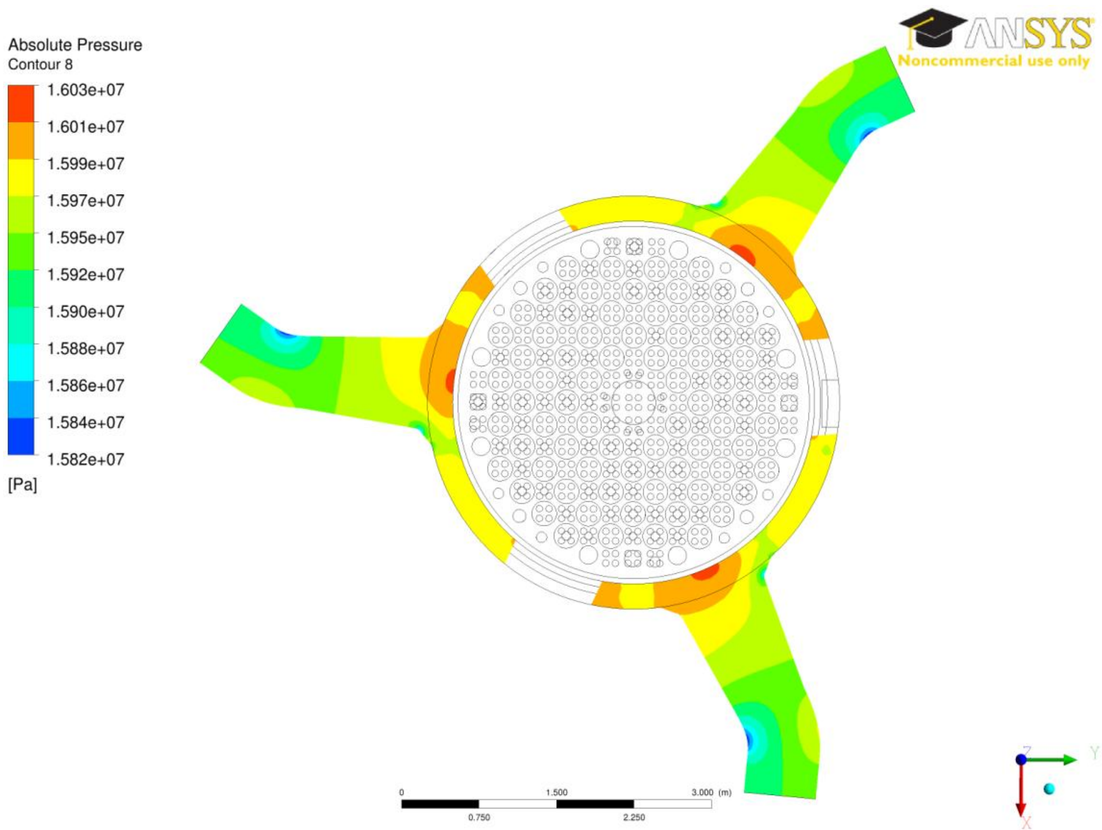

Figure D 6: Absolute pressure at the inlet height in the YX -plane